Downloaded from rsta.royalsocietypublishing.org

PHILOSOPHICAL TRANSACTIONS OF THE ROYAL SOCIETY A MATHEMATICAL, PHYSICAL & ENGINEERING SCIENCES

Channel Convection in Partly Solidified Systems

A. Hellawell, J. R. Sarazin and R. S. Steube

Phil. Trans. R. Soc. Lond. A 1993 **345**, 507-544
doi: 10.1098/rsta.1993.0143

Email alerting service

Receive free email alerts when new articles cite this article - sign up in the box at the top right-hand corner of the article or click **here**

To subscribe to *Phil. Trans. R. Soc. Lond. A* go to:
http://rsta.royalsocietypublishing.org/subscriptions

This journal is © 1993 The Royal Society

Downloaded from rsta.royalsocietypublishing.org

Channel convection in partly solidified systems

By A. Hellawell, J. R. Sarazin and R. S. Steube

Department of Metallurgical and Materials Engineering, Michigan Technological University, 1400 Townsend Drive, Houghton, Michigan 49931–1295, U.S.A.

Contents

	PAGE
1. Introduction	508
2. Previous work	511
3. Present work	515
(*a*) Objectives	515
(*b*) Material systems	516
4. Experimental methods and procedures	519
(*a*) Metals	519
(*b*) Aqueous system	520
(*c*) Organic systems	523
5. Results	524
(*a*) Global	524
(*b*) Microscopic dimensions	527
(*c*) Composition variations	528
(*d*) Plume temperature differences	531
(*e*) Plume flow rates	531
6. Discussion	532
(*a*) Mass balance	532
(*b*) Plume flow and analysis	533
(*c*) Selection of dimensions	535
(*d*) Entrainment and channel structure	536
7. Summary and conclusions	538
Appendix A. Mass balance and the fraction of NH_4Cl solid in the mushy zone	539
Appendix B. Plume flow with boundary movement	540
Appendix C. Helical plumes	541
References	543

Channel plume flow arising from thermosolutal convection has been examined in metallic, aqueous and organic systems, covering a range of Prandtl numbers over three orders of magnitude. Observations were made directly in the transparent aqueous and organic systems and after the event in fully solidified metallic alloys. Plume dimensions and those of the concomitant channels are remarkably similar in all three materials, as are the composition differences between plumes or channels and the matrices. Detailed measurements and observations of these dimensions and of flow rates in the transparent materials are described and discussed. Analysis of plume flow rates in the transparent systems, if extrapolated to metals, would predict convective flow rates between 0.1 m s^{-1} and 0.2 m s^{-1}. The validity of this

Phil. Trans. R. Soc. Lond. A (1993) **345**, 507–544
Printed in Great Britain

© 1993 The Royal Society

The Royal Society is collaborating with JSTOR to digitize, preserve, and extend access to *Philosophical Transactions: Physical Sciences and Engineering.* www.jstor.org

Downloaded from rsta.royalsocietypublishing.org

extrapolation is qualified by the way in which posthumous solute channels develop in the fully solidified metallic samples.

1. Introduction

During the solidification of metallic alloys which freeze over a significant temperature range, there can develop solute-rich channels which are left behind in a fully solidified ingot casting and which are recognized as serious casting defects. The channels develop in the partly solidified 'mushy' region of a casting and have dimensions of the order 1 mm in diameter, extending approximately vertically over distances exceeding 100 mm (Moore & Shah 1986). In billet castings of steel, with horizontal growth from vertical mould walls, they are termed 'A' segregates, lying almost vertically, but inclined inwards towards the billet axis, hence 'A'. With growth vertically upwards, as in electro-slag remelted (ESR) ingots, or in directionally solidified samples, such as turbine blades, they are identified as 'freckles', from their appearance on horizontal sections or on the outer surfaces, figure 1*a*, *b*. The principal solutes segregating within these channels are those which are less dense than the solvent metal, e.g. carbon, silicon, sulphur in steels, tin in lead, or aluminium and titanium in nickel base superalloys. The origin of the channels was identified in billet castings by Hunt (McDonald & Hunt 1969, 1970) as convection arising from the buoyancy forces caused by the segregation of less dense solutes within the partly solidified mushy region of a casting. The same effect was demonstrated shortly afterwards in base chilled configurations, with solidification vertically upwards, by Copley *et al.* (1970). In both these series of studies, the aqueous system NH_4Cl–H_2O was used as a transparent, visual analogue for metallic alloys: NH_4Cl crystallizes from aqueous solutions with a cubic, dendritic morphology, rejecting water as the less dense solute.

Convective plume or channel flow patterns (see later in this paper, figures 4, 5, 9 and 23) can be observed directly in the aqueous analogue and are strikingly similar in dimensions to those of segregation channels found by micro/macroscopic examination of fully solidified metallic samples, after the events which caused them. The plumes in the aqueous solution can be observed visually from refractive index changes with composition or enhanced by the introduction of dyes. Local flow rates of a few mm s^{-1} can be assessed from the latter and from the movement of small crystalline fragments or other solid particles. In opaque metallic alloys there are, as yet, no direct measurements of such flow rates and it has been the principal purpose of the work described in this paper to extrapolate measurements from transparent materials to make reasonable estimates of flow rates which might be expected in metals.

Natural convection occurs when density differences arise in different parts of a system from both temperature (T) and/or composition (C) variations. The thermal and solutal density gradients are determined by the corresponding coefficients of volume expansion with temperature and composition, α and β; where α is positive but β may have either sign and they are only coincidentally the same numerically. Of particular interest are geometrical situations where the vertical density gradients, $d\rho/dz$, with respect to temperature, T, and composition, C, are not only unequal to each other, but are also of opposite sign, particularly when $-(d\rho/dz)_T < (d\rho/dz)_C$.

Such situations develop during both solidification and melting, and may arise

PHILOSOPHICAL TRANSACTIONS OF THE ROYAL SOCIETY A MATHEMATICAL, PHYSICAL & ENGINEERING SCIENCES
PHILOSOPHICAL TRANSACTIONS OF THE ROYAL SOCIETY A MATHEMATICAL, PHYSICAL & ENGINEERING SCIENCES

Downloaded from rsta.royalsocietypublishing.org

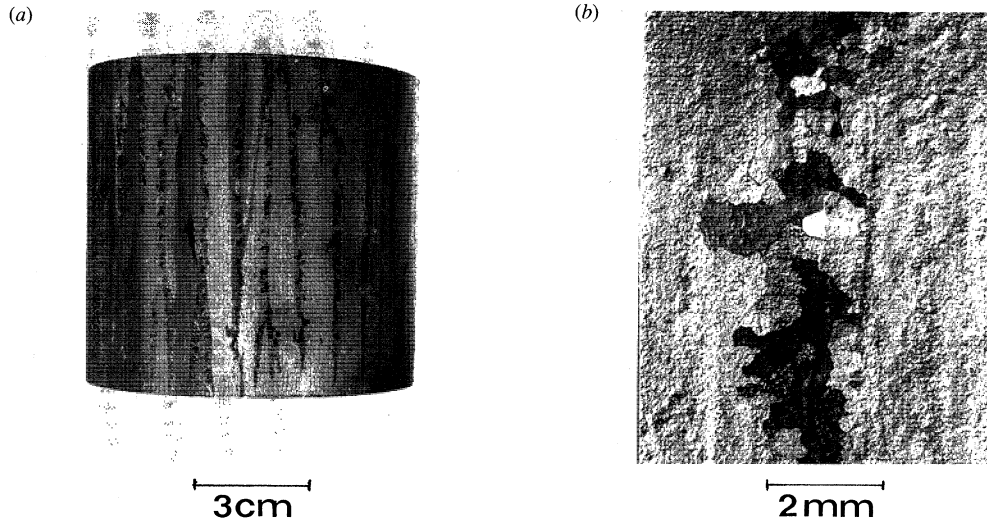

Figure 1. Deeply etched surface of a directionally solidified, superalloy ingot showing severe 'freckle' formation, (*a*) macroscopic view and (*b*) detail. Courtesy A. F. Giamei, United Technologies Research Center.

adjacent to a planar solid–liquid interface (Sharp *et al.* 1972; Coriell *et al.* 1980; Hurle *et al.* 1982; Fang *et al.* 1988), or when there exists a two-phase solid–liquid volume – a so-called 'mushy zone' – as within a partly solidified ingot freezing over a temperature range. The present work is concerned with the latter situation during solidification. It concerns systems in which the solid phase is non-faceted, growing with a dendritic morphology to form a regular, uniformly spaced geometrical array of solid spines with side branches, generally growing normal to the direction of heat removal. Materials which can solidify in this manner have low entropies of fusion or solution and include metallic alloys, some simple ionic salts growing from the melt, a limited number of inorganic aqueous systems, and a few organic materials having non-polar, symmetrical molecules. Reference will be made to all of these.

Clearly, subject to the direction of heat removal, growth may be constrained to take place at any inclination to the gravitational vector into a positive temperature gradient. The principal concern here will be with that configuration where the heat flow is vertically downwards and growth occurs antiparallel to the gravitational vector. This is in some ways the experimentally and analytically most tractable configuration.

We refer to figure 2 for a binary alloy system. In figure 2*a*, a solute depresses the freezing point of a component; the liquidus slope, $\delta T/\delta C$, is negative and the solid/liquid distribution coefficient, $k_0 = C_{\mathrm{d}}/C_{\mathrm{L}} < 1$. The situation is considered where the prevailing growth rate, V, imposed positive, vertical temperature gradient, $\delta T/\delta z$, and alloy composition, C_0, are such as to allow the development of a dendritic growth front and a significant (e.g. $\gtrsim 10$ mm deep) solid–liquid 'mushy zone'. In figure 2*b*, it lies below a volume of supernatant liquid of initial composition C_0, and above a region where the material is fully solid, as below some terminal eutectic temperature in the phase diagram.

Above the dendritic growth front the combination of a positive temperature gradient and thermal coefficient of expansion leads to a negative density gradient, $(\mathrm{d}\rho/\mathrm{d}z)_{\mathrm{T}}$, and the bulk liquid is stabilized against convection.

PHILOSOPHICAL TRANSACTIONS OF THE ROYAL SOCIETY A MATHEMATICAL, PHYSICAL & ENGINEERING SCIENCES
PHILOSOPHICAL TRANSACTIONS OF THE ROYAL SOCIETY A MATHEMATICAL, PHYSICAL & ENGINEERING SCIENCES

Downloaded from rsta.royalsocietypublishing.org

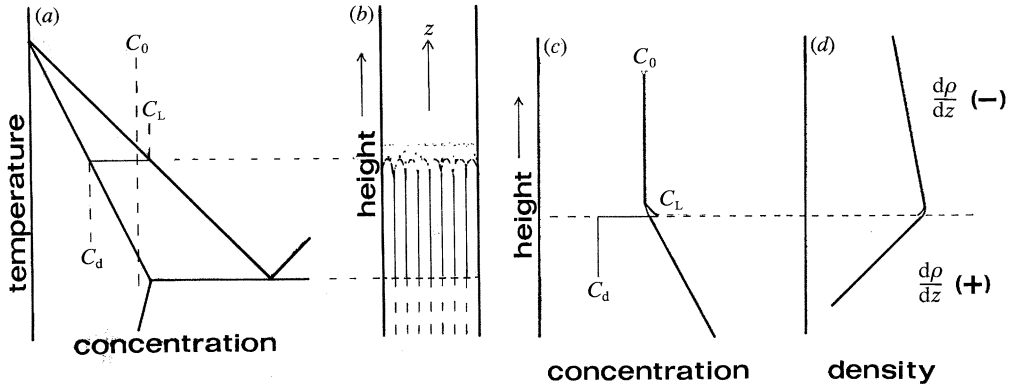

Figure 2. (*a*) Relevant region of a phase diagram. Initial liquid composition, C_0; interfacial boundary composition, C_L, depositing dendrites of tip composition, C_d. (*b*) Corresponding experimental configuration in a vertical temperature gradient, dT/dz. (*c*) Composition profiles, corresponding to (*a*) and (*b*). (*d*) Corresponding density profile for the liquid above and below the plane of the dendritic growth front.

Immediately above the growth front, figure 2*c*, is a small solute boundary layer of maximum composition C_L, from which grow dendrites with a tip composition C_d. Below the growth front the interdendritic liquid composition increases according to the phase diagram and reciprocal liquidus slope,

$$\frac{\delta C}{\delta z} = \frac{\delta C}{\delta T} \times \frac{\delta T}{\delta z}.$$

Now, if the solutal expansion coefficient, β, is positive, it is then possible that below the front the vertical liquid density gradient, corresponding to that along the liquidus composition, i.e.

$$\frac{\delta \rho}{\delta z} = \frac{\delta \rho}{\delta C} \times \frac{\delta C}{\delta z},$$

may be positive, as in figure 2*d*.

There is then density inversion at and below the growth front and the system is inherently unstable. If the relative magnitudes of the expansion coefficients, the liquidus slope and temperature gradients are such that the positive density gradient below the front exceeds the negative gradient above it (i.e. $\alpha\,\delta T/\delta z < -\beta\,\delta C/\delta z$), It might be expected that the solutal buoyancy would be sufficient to cause some form of convection to reduce the potential energy of the system. However, to cause a perturbation, leading to 'thermosolutal' convection, requires also that the excess buoyancy be sufficient to overcome the inertia of the fluid, limited by the viscosity and thermal conductivity. This is a modified or thermosolutal version of the Bénard–Rayleigh problem (Turner 1973, 1985; Huppert & Turner 1981).

As is obvious from the above, thermosolutal convection is a generic phenomenon, being widely recognized in oceanographic contexts as 'thermo-haline' convection, and in the geological context of molten magma chambers (see Turner 1985). Oceanographic salt fingers or fountains can arise between layers of aqueous solution of different concentrations (Stern 1960) and can be caused by the melting of icebergs in sea water (Huppert & Turner 1980). In magma chambers, compositional variations can similarly develop during solidification or melting (Spera 1980; Huppert & Turner 1981). The phenomenon can in principle occur whenever there

Downloaded from rsta.royalsocietypublishing.org

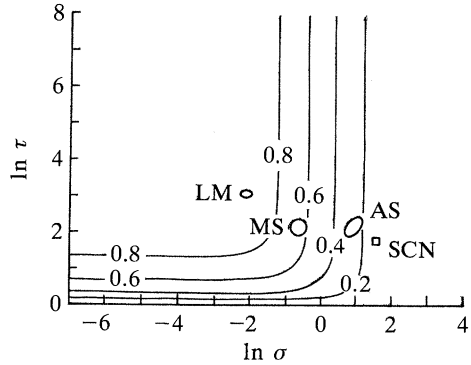

Figure 3. Plot of $\ln \tau$ (diffusivity ratio, κ/D_L, or Lewis number) versus $\ln \sigma$ (Prandtl number, ν/κ) showing positions corresponding to various materials. LM, liquid metals; MS, molten salts; AS, aqueous salts; SCN, molten succinonitrile. The inset contours correspond to a dimensionless flow velocity. After Schmitt (1983).

arise different transport processes between two species (i.e. heat and matter), and depends upon the ratio of the respective diffusivities, κ and D_L, the Lewis number, τ, and upon the Prandtl number, σ, the ratio of the kinematic viscosity, ν, to the thermal conductivity, κ. Schmitt (1983) has shown that different material systems can be conveniently grouped in terms of these two dimensionless numbers, τ and σ, and in terms of these numbers a given class of materials (metals, aqueous solutions, etc.) falls within a relatively small and discrete area, figure 3. Indicated here are the ranges corresponding to liquid metals (LM), molten salts (MS), aqueous solutions (AS) and molten succinonitrile (SCN) as an organic compound which freezes with a dendritic, non-faceted morphology. As may be seen, the Lewis numbers for these examples do not differ widely, but the Prandtl numbers cover a range of three orders of magnitude, from *ca.* 2×10^{-2} in metals to *ca.* 20 in the organic case. In the original figure, Schmitt considered a wider range of examples to include molten magmas, heat and water vapour in a meteorological context, and also superimposed a series of contours for a dimensionless velocity, increasing with decreasing Prandtl number and with increasing Lewis number. The question will arise as to whether convection patterns and models may be extrapolated across wide ranges of Prandtl or Lewis numbers, but the apparent similarity in channel segregation patterns between metals and aqueous systems (and, as it transpires, in organic materials) would suggest that such extrapolation is justified; but, as previously noted, there are no measured velocities for channel flow in metals.

2. Previous work and the present context

The basic situation is one where there exist two layers of fluid, the lower of which is less dense than the other, having a higher concentration of a less dense component. This is the situation which occurs in an oceanographic context and which has been the subject of extensive experimental and mathematical study during the past 30 years (e.g. Stern 1960, 1969; Turner 1973; Huppert & Turner 1981; Holyer 1981, 1983, 1984; Turner 1985; Veronis 1987; Howard & Veronis 1987; Chen *et al.* 1971; Bennon & Incropera 1987; Chen & Chen 1988). The situation under consideration here differs in several ways.

(i) The lower liquid layer is constrained within a regular array of solid spines,

PHILOSOPHICAL TRANSACTIONS OF THE ROYAL SOCIETY A MATHEMATICAL, PHYSICAL & ENGINEERING SCIENCES
PHILOSOPHICAL TRANSACTIONS OF THE ROYAL SOCIETY A MATHEMATICAL, PHYSICAL & ENGINEERING SCIENCES

Downloaded from rsta.royalsocietypublishing.org

dendrites, the periodicity of which is predetermined during solidification by the growth rate, imposed temperature gradient and alloy concentration within a given system.

(ii) The geometrical configuration, cf. figure 2, is one where the sample lies in a positive vertical temperature gradient so that the initial densities of the two liquid reservoirs are not constant but exhibit gradients of opposite signs, as in figure 2*d*. This also means, with reference to the phase diagram, figure 2*a*, that the volume fraction of interdendritic liquid decreases continuously below the plane of the dendritic growth front.

(iii) As heat is continuously removed from the base of the sample, the growth front moves upwards and the composition of the interdendritic liquid is continuously replenished by the phase change. With convective mixing, the composition of the supernatant liquid rises continuously.

(iv) As solidification proceeds from an approximately constant base temperature, the vertical temperature gradient and the growth rate decrease continuously. Subject to the efficiency of heat removal the sample may or may not solidify completely. (In metallic systems, with freezing points above ambient temperatures, solidification is eventually complete, but in aqueous and organic systems with eutectic temperatures below 0 °C, solidification may not be complete.)

It is important to distinguish between *two convective régimes*.

(*a*) Starting soon ($\gtrsim 30$ s) after the development of a dendritic growth front, there occurs a fine-scale 'finger' type of convection immediately above the growth front. This involves fluctuating emissions of the less dense, solute-rich fluid as fingers, having diameters comparable to the primary dendritic spacing (e.g. < 0.5 mm) and rising eventually to some 5 mm above the growth front. Such fingers are observed in the aqueous system NH_4Cl–H_2O (Sample & Hellawell 1984) in the organic system succinonitrile–ethanol, SCN–EtOH (this work), and there is some evidence of their prior existence in metallic samples at higher solute contents where the dendritic mesh is more open (Sarazin & Hellawell 1988). This régime is similar to that described between two unconstrained fluid layers (Huppert & Turner 1981) in which the rising liquid fingers are balanced by downward flow from the upper, more dense reservoir, to give an approximately square wave pattern (Veronis 1987; Howard & Veronis 1987). In the present context, however, the pattern develops above the periodic array of a dendritic front and therefore is constrained to develop with a wavelength which is to some extent independently predetermined. The wavelength selection for these perturbations will not necessarily be the same as for the unconstrained case, although the dimensions may be similar, because both the dendritic spacing and finger diameters are related to the solutal diffusion coefficient. This finger régime develops across the entire growth front over all composition ranges for which there is a mushy zone.

(*b*) Within restricted composition ranges and certain solidification conditions, larger-scale convection patterns can develop in the form of solute plumes or chimneys (McDonald & Hunt 1969, 1970; Copley *et al.* 1970) having diameters of up to some five primary interdendritic spacings and rising through the supernatant liquid to heights in excess of 100 mm. When these develop (typically when the mushy zone is $\gtrsim 5$ mm in depth, at longer times, $\gtrsim 10$ minutes), they completely replace the short-range 'finger' régime, and, as they do so, release larger volumes of interdendritic liquid, causing local channels to develop in the mushy zone. These are thought to be the cause of the channel segregation defects previously referred to in

PHILOSOPHICAL TRANSACTIONS OF THE ROYAL SOCIETY A MATHEMATICAL, PHYSICAL & ENGINEERING SCIENCES
PHILOSOPHICAL TRANSACTIONS OF THE ROYAL SOCIETY A MATHEMATICAL, PHYSICAL & ENGINEERING SCIENCES

Downloaded from rsta.royalsocietypublishing.org

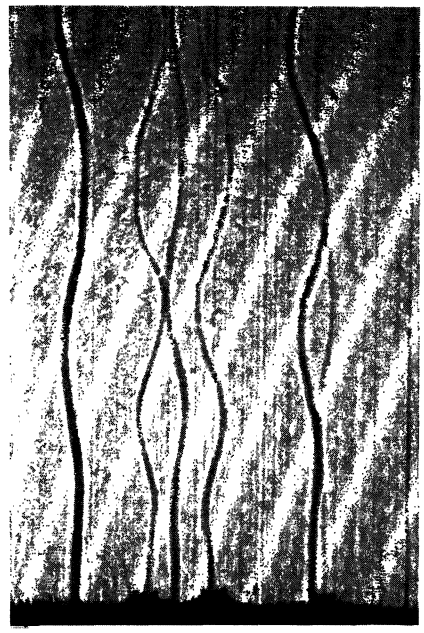

Figure 4. General view of plumes in NH_4Cl–70 wt% H_2O soon (*ca.* 20 min) after their formation. Width of cell is 48 mm. Vertical streaks are from acrylic mould.

Figure 5

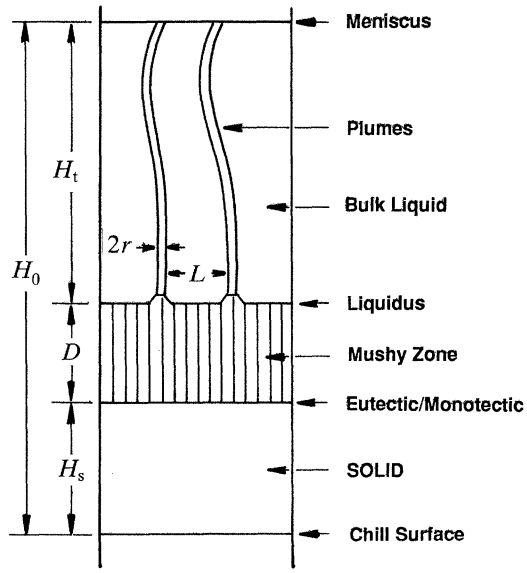

Figure 5. Schematic diagram for figure 4 to show the dimensions considered in this text.

metal castings. We believe that these larger-scale plumes are the equivalent of the 'salt fountains' in oceanographic contexts, but are not certain of this parallel. Figure 4 shows such plumes in a NH_4Cl–H_2O casting, and figure 5 is a schematic diagram including some dimensions which will be considered in this work.

Downloaded from rsta.royalsocietypublishing.org

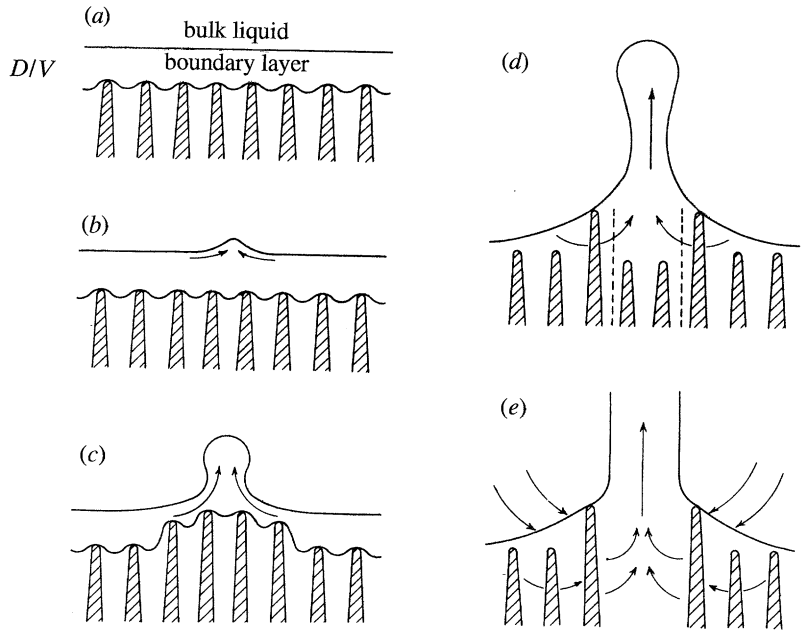

Figure 6. Schematic representation of boundary layer perturbation leading to plume and channel formation. Note that the entrainment of bulk liquid must first accelerate the dendritic growth front locally, as observed (Hellawell 1987), while the release of solute-rich liquid from below causes subsequent melting, in the order (*a*)–(*e*).

Inasmuch as the 'finger' régime always precedes, but is superseded by, the plume régime, if it occurs, the 'fingers' may be regarded as precursors to the plumes, but the transition from one régime to the other must involve coupling not only between the upper level of the finger zone and the quiescent reservoir above, but also at the lower level, adjacent to and below the level of the dendritic growth front. It will be assumed, in this paper, that the plume development or 'nucleation' arises from a liquid perturbation at or close to the level of the growth front, as depicted schematically in figure 6, corresponding to that region, cf. figure 2*d*, where there is a change in the sign of the vertical density gradient. There is ample experimental evidence (e.g. Sample & Hellawell 1982, 1984; Sarazin & Hellawell 1988; Hellawell 1987, 1990) to support this view. We do not think that alternative attempts to model channel development in a global sense, from positions within the mushy zone itself, are physically realistic (Voller & Moore 1983; Simpson *et al.* 1985; Bridge *et al.* 1982; Kawamuri *et al.* 1988; Chen & Chen 1988; Pagalthivorthi & Desai 1986; Bennon & Incropera 1987; Poirier 1987). This is not to imply that the dimensions of the mushy zone are unimportant, because channel plumes occur only in limited composition ranges; see phase diagrams, figure 7*a–d*. The dimensions (spacings) of the dendritic array and the openness or permeability of the upper mushy zone are obviously important in allowing plumes to develop, but the initial perturbation must originate in the open liquid above the growth front. In conclusion, it should be noted that the above comments relate specifically to the vertical configuration, at and above a horizontal growth front. One must be aware that in other configurations there will be thermal or solutal convective flows across the growth front which complicate the situation considerably and can preclude plume convection or restrict finger patterns (McDonald & Hunt 1969, 1970; Copley *et al.* 1970; Sample & Hellawell 1982).

Downloaded from rsta.royalsocietypublishing.org

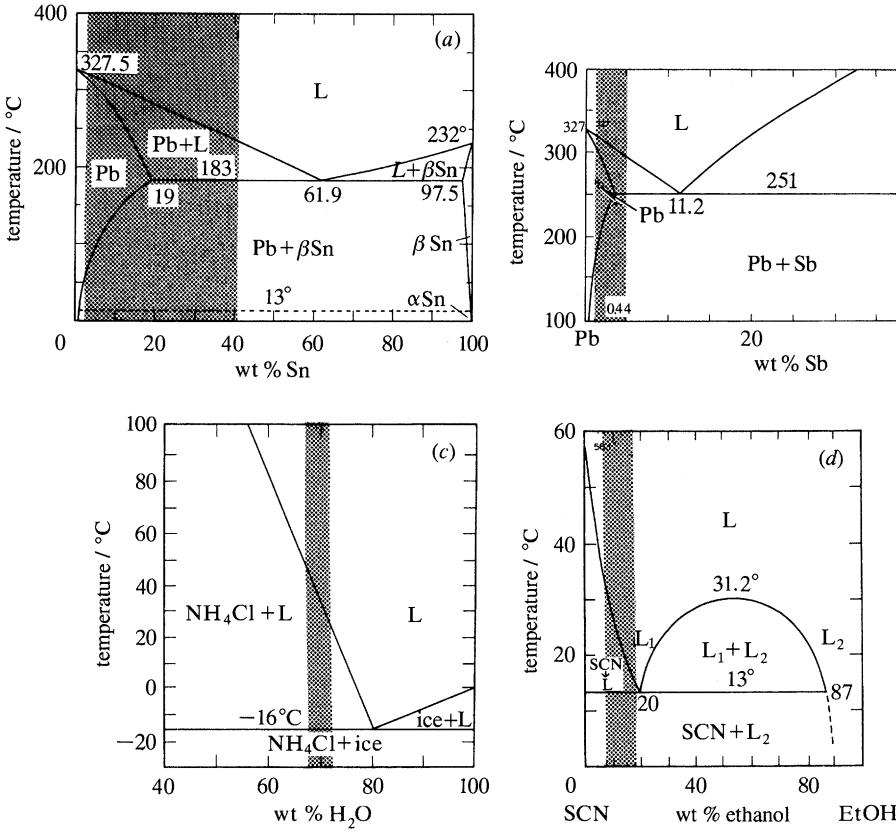

Figure 7. Phase diagrams of parts thereof with relevant composition ranges shaded: (*a*) Pb–Sn; (*b*) Pb–Sb; (*c*) NH_4Cl–H_2O; (*d*) SCN–EtOH.

Finally, it is important to emphasize that the present work and discussion originates in a metallurgical context and concerns materials which solidify with a non-faceted, dendritic morphology of given periodicity. It does not automatically follow that the convective patterns adjacent to faceted crystals will develop in exactly the same way, because the same permeable and periodic mushy zones are absent in such cases.

3. Present work

(*a*) *Objectives*

As explained, the primary concern is with quasi-steady-state plume flow, as in figure 4, which is sustained by the continuous progress of the phase change and recirculation of bulk supernatant liquid through the upper levels of the mushy region adjacent to channel exits or 'mouths'. The object has been to obtain quantitative measurements relating to such plume flow in transparent systems and to examine how far these can be extrapolated to behaviour in metals. The data which are relevant to an analysis and comparison can be identified by reference to figure 5; these now follow.

(i) Global dimensions: the height, H_t, of the bulk liquid above the dendritic growth front and the depth, D, of the permeable mushy zone below that level and

Downloaded from rsta.royalsocietypublishing.org

down to that of the terminal eutectic (or other) front. Also over this range, the vertical temperature gradients, $\delta T/\delta z$, and the related growth rates of the dendritic and eutectic fronts; hence the timescale.

(ii) Microscopic dimensions: the average interdendritic spacing, λ; the effective radius of plumes or channels, r; and the spacing between plumes/channels, L.

(iii) The compositions of the bulk liquid or matrix, C_L, at given times and positions, and those of the plumes or channels (measured post mortem in metals); hence, the composition differences, ΔC, between plumes/channels and the bulk.

(iv) In the transparent materials, the plume and bulk liquid temperatures as a function of position (height above the growth front), and therefore the temperature differences, ΔT, between these, and the bulk liquid.

(v) The mean, visual, plume flow velocities, $\bar{v}$, as functions of the time and position, observed directly in the transparent materials.

A summary of these measurements is given in table 2, § V of this paper. No attempt has been made to carry out measurements of similar quantities for the finer scale, transitory 'finger' régime.

(*b*) *Material systems*

The relevant phase diagrams or portions thereof are shown in figure 7*a–d*. On these diagrams, the shaded regions indicate the ranges of composition which were examined in the present work although channel/plume convection is not necessarily restricted to these ranges. Table 1 contains information about these phase diagrams, some relevant physical properties, and derived quantities or numbers. Some comments about these and other systems are in order:

(i) *Metallic alloys, lead–tin and lead–antimony: figure* 7*a–b*

The composition ranges of interest are on the lead-rich sides of the eutectic points. Tin and antimony are significantly less dense than lead and therefore provide solutal buoyancy effects. Detailed studies of channel segregation in these binary systems and of ternary Pb–Sb–Sn alloys were made by Sarazin & Hellawell (1988). The systems differ from the aqueous and organic systems in having significant solid solubility in lead, so that there occurs some fractional segregation within the solid phase, requiring modification of the lever rule by the Scheil equation (1942) to calculate phase fractions below the liquidus temperature. It may also be noted that in the metallic systems, having high thermal conductivities and low Prandtl number, channel convection occurs at relatively lower solute ranges than it does in the poorly conducting non-metallic systems. This also means that channel/plume formation takes place from within/above a mushy zone in which the liquid fraction is lower (i.e. is less permeable) than it is in the other systems.

(ii) *Aqueous ammonium chloride, NH_4Cl–H_2O: figure* 7*c*

This is a simple eutectic system with negligible solid solubility on either side; ammonium chloride forms no hydrated compounds. Wider compositional ranges than that shaded have been examined previously (e.g. Sample & Hellawell 1982, 1984) but in any case, there is an experimental limitation in that the solution boils at *ca.* 55 wt% H_2O. For the purposes of the present work, pouring solutions into moulds with sufficient superheat to avoid general equiaxed crystal formation, the practical upper limit of NH_4Cl concentration is therefore *ca.* 35 wt% (65 wt% H_2O). This means that it has not been possible to determine the lower limit of solute (H_2O)

Downloaded from rsta.royalsocietypublishing.org

Table 1. *Quantities used in text*

	metallic Pb–10 wt % Sn	aqueous NH_4Cl–70 wt % H_2O	organic SCN–15 wt % EtOH
derived data from phase diagrams			
liquidus slope, dT/dC, K wt %	−2.2	−4.8	−3.6
solid–liquid distribution coefficient, C_S/C_L	0.30	0.0	0.04
weight fraction liquid, f_L, at eutectic/monotectic temperature	0.08	0.86	0.74
physical properties			
thermal diffusivity, κ, of liquid ($m^2\ s^{-1}$)	1.08×10^{-5}	1.47×10^{-7}	1.12×10^{-7}
solutal diffusivity D_L, of liquid ($m^2\ s^{-1}$)	3×10^{-9}	1.3×10^{-9}	1.0×10^{-9}
liquid density, ρ ($kg\ m^{-3}$)	1.01×10^4	1.08×10^3	9.52×10^2
dynamic viscosity, η ($kg\ m^{-1}\ s^{-1}$)	2.47×10^{-3}	1.03×10^{-3}	2.56×10^{-3}
volume thermal expansion coefficient, α (K^{-1})	1.16×10^{-4}	4.0×10^{-4}	8.1×10^{-4}
volume solutal expansion coefficient, β (wt %$^{-1}$)	5.2×10^{-3}	2.5×10^{-3}	2.3×10^{-3}
refractive index, μ			
(i) thermal coeff., $d\mu/dT$ (K^{-1})	—	-1.7×10^{-4}	-2.8×10^{-4}
(ii) solutal coeff., $d\mu/dC$ (wt %$^{-1}$)		-1.8×10^{-3}	-5.2×10^{-4}
volume changes on freezing, % $\Delta V/V$			
(i) primary dendrites	−3.5	−35	−6
(ii) eu(mono)tectic	−3.0	+7	−4
derived quantities			
kinematic viscosity, $\nu = \eta/\rho$ ($m^2\ s^{-1}$)	2.43×10^{-7}	9.54×10^{-7}	2.69×10^{-6}
Lewis number, κ/D_L	3.6×10^3	1.07×10^2	1.12×10^2
Prandtl number, ν/κ_L	2.3×10^{-2}	6.8	21.5

concentration for channel/plume convection, but it is notable that it occurs much closer to the eutectic point than is the case in metallic alloys. The density difference between solid NH_4Cl and solution is large (*ca.* 35%) compared with the other systems, so that with the form of the phase diagram, even with some vertical macroscopic segregation during the solidification of a casting, the solid fraction in the mushy region is very low and it is therefore very open or permeable in the practical range of interest. Some estimates of the solid : liquid fractions are made later in this paper; see §6 and Appendix A.

In this, as in many systems, it is possible to make ternary additions which adjust the solutal expansion coefficient, β, and allow of certain compositions where β tends to zero, although as solidification proceeds and composition changes, it is not possible to remain at the isodensity point. Such adjustments were made to the NH_4Cl–H_2O system by additions of zinc chloride to reverse the sign of the solutal coefficient (McDonald & Hunt 1970) and a partial ternary phase diagram was determined by Sample (1984), but convection is remarkably sensitive to small composition changes

Downloaded from rsta.royalsocietypublishing.org

(Fisher & Hunt 1977) and the dendritic morphology may also change (Sarazin 1990). Results in ternary systems will not be considered in the present paper.

(iii) *Organic system: succinonitrile–ethanol* ($NCCH_2CH_2CN$–C_2H_5OH) *or* SCN–EtOH*: figure* 7*d*

This system may require qualification inasmuch as the reaction taking place at a lower temperature occurs at a monotectic rather than eutectic isotherm, i.e. the reaction is of the form, liquid $L_1 \Leftrightarrow$ solid SCN + liquid L_2, so that solidification is still not complete below that temperature. This is not thought to be a significant problem in the present context, because the minor, ethanol-rich product of the reaction, L_2, is incorporated in solid, SCN, within fine irregular tubes and cavities (Grugel *et al.* 1984). This ethanol-rich liquid is immiscible with the parent liquid phase and, although less dense, cannot easily be released from the monotectic growth front within the composition range of interest. The nature of this reaction is not therefore relevant to the convection at higher levels.

The phase diagrams for other binary systems between SCN–H_2O and other alcohols are of similar form to that with ethanol, with continuous miscibility gaps and monovariant reactions across ternary systems (Schreinemakers 1898; Grugel *et al.* 1983; Kaukler & Frazier 1985). Thus, in the ternary system SCN–EtOH–H_2O, it is possible to vary the solutal buoyancy continuously to near zero in the SCN–H_2O system. Some observations of ternary solutions were made in the course of this work, but were somewhat ambiguous because the dendritic morphology also changed with composition and will not be considered further in this paper.

Particular attention is drawn to the range of Prandtl numbers for these materials (table 1) referred to previously, and to the wide range of two orders of magnitude between metals and aqueous systems. In this respect it would be very satisfactory were it possible to perform some parallel experiments with molten, anhydrous inorganic salts, which have Prandtl numbers around *ca.* 5×10^{-1}, thus reducing the range of extrapolation. Moreover, such materials have an added experimental advantage in that they are transparent and can be observed directly within glass or quartz containers and can further be examined when fully solidified by microscopy and conventional solid state analytical methods, such as electron microprobe analysis.

However, inspection of thermal and solutal density coefficients (Smithells 1976) and phase diagram data (Levin *et al.* 1964, and supplements) reveals that the solutal buoyancy contributions are frequently too small to outweigh the thermal density gradients in those systems which are experimentally tractable and also in which a dendritic, as opposed to a faceted, morphology develops. Moreover, even when the buoyancy contribution, depending on $\beta\,\delta c/\delta z$, exceeds the corresponding thermally stabilizing gradient, $\alpha\,\delta T/\delta z$, the difference is often insufficient to overcome the inertial terms and the outcome has been a frustrating lack of comparative behaviour: nature is perverse.

In the following section, experimental methods are described for the different materials; the results are described with reference to the measurable quantities in §5; and these are analysed and discussed in §6.

PHILOSOPHICAL TRANSACTIONS OF THE ROYAL SOCIETY A MATHEMATICAL, PHYSICAL & ENGINEERING SCIENCES
PHILOSOPHICAL TRANSACTIONS OF THE ROYAL SOCIETY A MATHEMATICAL, PHYSICAL & ENGINEERING SCIENCES

Downloaded from rsta.royalsocietypublishing.org

4. Experimental methods and procedures

(*a*) *Metals*

Lead base alloys with tin and antimony were examined. The details of the basic procedure have been described elsewhere (Sample & Hellawell 1984; Sarazin & Hellawell 1988) but were essentially as follows: The alloys, in ranges from 5 wt% Sn to 40 wt% Sn and from 1 wt% Sb to 5 wt% Sb, were prepared by melting together the components, having purities $\gtrsim 99.9$ wt%. For the present purposes, higher purities were unnecessary, and tin and antimony are, in any case, among the principal impurities in lead. The alloy melts, weighing 1.5 kg, were poured at 500 °C into hot graphite moulds of 38 mm ID and 200 mm high, situated within a resistance furnace and standing upon a water-cooled base. The furnace was then cooled at a programmed rate of 0.5 K min^{-1} from 500 °C to below the relevant eutectic temperature (see phase diagrams, figure 7*a*, *b*). A full thermal record was taken of representative samples by a series of chromel–alumel thermocouples set within the sample at vertical intervals of 20 mm. The thermocouple outputs were interfaced with a computer to provide detailed records of thermal gradients against position and time. The fully solidified ingots were then extracted from the mould and sectioned vertically, diametrically, and horizontally at 20 mm intervals.

Metal filings were taken from one surface of each horizontal section and were chemically analysed by atomic absorption spectroscopy. This compositional data, combined with the thermal data using the phase diagrams, provided interfacial positions as a function of time and hence growth rates with time and position.

Complete solidification occurred over time periods between 6 and 8 h, subject to composition and system. Growth rates and temperature gradients changed with time and position, the former initially decreasing from *ca.* 10 to *ca.* 5 μm s^{-1} and then increasing again over a similar range, while the latter decreased with time and height from *ca.* 1 to *ca.* 0.2 K mm^{-1} in the vicinity of the growth front.

Microscopical examination of sections was carried out using standard procedures and yielded average primary interdendritic spacings, measured from the number per unit area, the reciprocal square root of which corresponds to the sides of the square grid pattern of the dendritic mesh (see Sample & Hellawell 1984; Sarazin & Hellawell 1988).

The same sections were used to assess the effective channel diameters from etching contrast, and in the polished condition to provide samples for detailed chemical analysis using electron microprobe analysis (EMPA).

EMPA was used to measure the local solute concentration across channels and into the dendritic array on either side. To reduce the 'noise' caused by local interdendritic segregation and within the channels themselves, the electron beam was adjusted to a line scan of *ca.* 1 mm, the orientation of which was rotated so that it was normal to the appropriate collimator and analyzing crystal for the radiation concerned. The sample movements were then programmed so that these followed a line trace at right angles to the beam scan in steps of 33 μm, thus sweeping out an area. An example of such an area scan is shown in figure 8 for a channel in a Pb–2 wt% Sb sample; the channel is discernible from the back scatter image as an area containing larger regions of the Pb–Sb eutectic and the probe line scans are apparent as parallel burn lines.

Such analyses were carried out on a number of channels in a given section and selected channels were also followed on successive sections at increasing heights

Downloaded from rsta.royalsocietypublishing.org

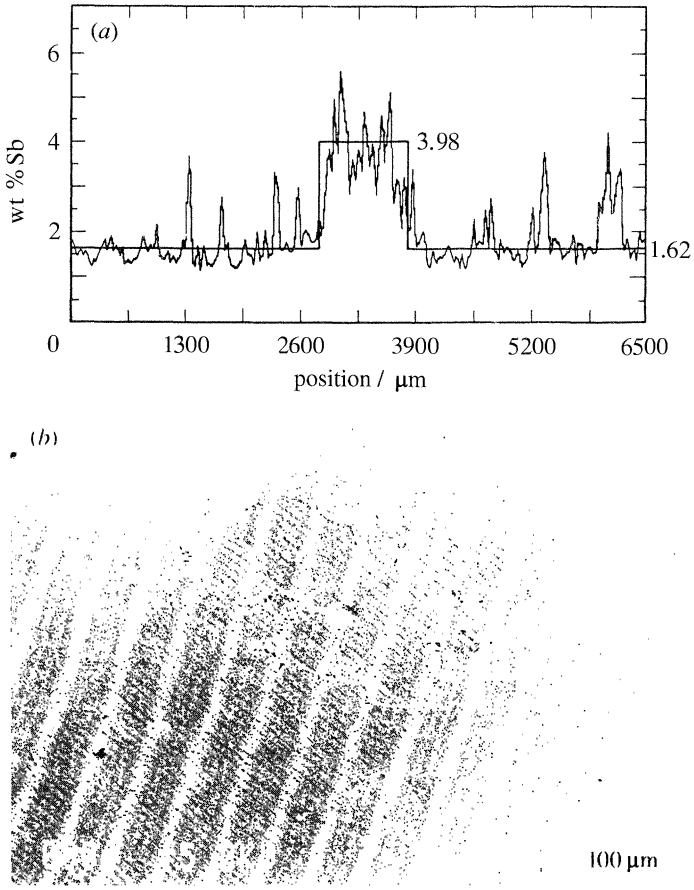

Figure 8. (*a*) EMPA area scan across a segregation channel in a Pb–2 wt % Sb sample, and (*b*) the corresponding back scatter image showing pockets of eutectic material and the line scan traces at 33 μm intervals.

along the samples in the growth direction. On a typical analytical trace, as in figure 8, the points were averaged in groups of three and the channel boundaries were identified and correlated with the back scatter image. To obtain the composition differences, ΔC, the results were averaged across the channel and within the matrix. As may be seen from the microstructure and analyses, precise channel boundaries are difficult to define and, in any case, channel sections are not perfectly circular, so that the choice of radius is necessarily somewhat subjective to within $\pm 10\,\%$.

(*b*) *Aqueous system:* NH_4Cl–H_2O

The binary aqueous system has been widely used as a transparent analogue for metallic alloy solidification studies (e.g. Jackson *et al.* 1966; McDonald & Hunt 1969, 1970; Copley *et al.* 1970; Sample *et al.* 1982, 1984). A variety of experimental 'moulds' have been used, according to the aspects of solidification under study, e.g. simulated castings with side chill or base chill, as in this work. The procedures are fairly standard, whereby hot ammonium chloride solutions are poured into a transparent container which is cooled by copper sides or bases which are partially immersed in a refrigerant. In this study the arrangement involved square section acrylic or pyrex tubing of inside width 50 mm and height 200 mm, sealed onto a

Downloaded from rsta.royalsocietypublishing.org

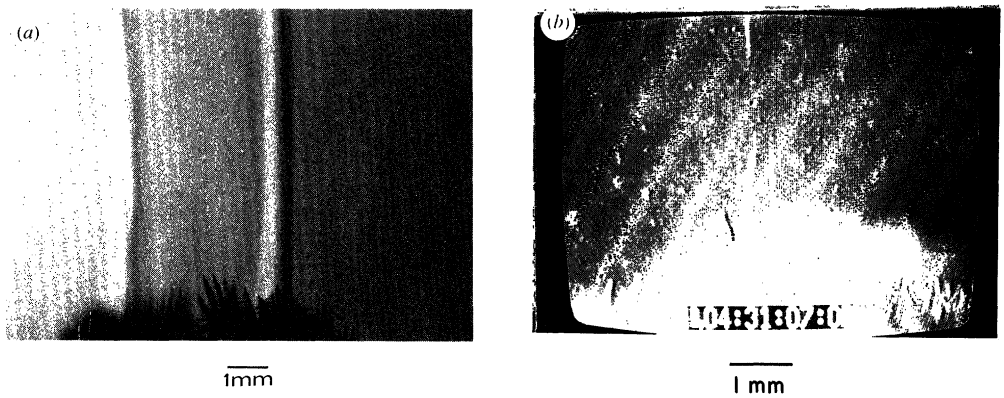

Figure 9. Channel mouth(s) with concomitant plume flow in a NH_4Cl–70 wt % H_2O casting after *ca.* 1 h; (*a*) light field image and (*b*) dark field image from video screen. In (*a*), the plumes (two, adjacent) are distinguished by sharp, concentration-dependent steps in refractive index; in (*b*), plume flow is detectable by particulate trajectories.

copper base, which in turn was soldered onto a copper tube immersed in a large (2 l) Dewar containing liquid nitrogen (−196 °C) at a constant level, with necessary insulation to reduce condensation around the copper base from the atmosphere. Some taller and shorter samples were also examined in moulds of height 1 and 0.1 m to examine effects caused by the upper meniscus. In the former, the upper regions were warmed by radiant heat to delay precipitation of crystals at longer times; in the latter, samples solidified completely after some 3–4 h.

In the present work, solutions were prepared containing from 65 wt % H_2O to 75 wt % H_2O; as may be seen on the phase diagram, figure 7*c*, this range corresponds to freezing intervals between the liquids and eutectic horizontal from *ca.* 50 K to −16 K. All solutions were poured from 80 °C. The majority of the present studies related to a 70 wt % H_2O solution.

Visual studies were made from the side and top of the mould using fibre-optic illumination, also using a shadow projection onto a translucent screen from a point light source. The contrast in such images is caused by variations in refractive index with composition and, to a minor degree, with temperature. Thus, for aqueous ammonium chloride the solutal coefficient of refractive index is 1.8×10^{-3} wt %$^{-1}$, while the thermal coefficient is 1.7×10^{-4} K^{-1}. With water as the solute, the interiors of plumes have a slightly lower refractive index than the bulk solution. In fact, the composition profile is essentially a step function across a plume, but the velocity profile is smeared out. The visual contrast is determined by composition, figure 9*a*.

More detailed examination of the growth front and channel/plume convection was made using a binocular microscope with a 1× apochromatic long working distance objective. Visual records were made through this microscope by a videotape recorder at frame intervals of $\frac{1}{30}$ s, and these, with optical magnification, when displayed upon a television screen gave a magnification of up to 100×. With a working distance of 90 mm, the depth of field was *ca.* 70 mm, the field width *ca.* 17.5 mm, and gave a resolution $\gtrsim 20$ μm. The plumes were then detected, either from changes in refractive index or by the movement of a high density ($\gtrsim 10$ mm^{-3}) of small crystalline dendrite fragments, figure 9*b*. This arrangement allowed detailed measurements of flow rates to be made by tracing the positions of particles on successive frames of the video record. The particles were small dendritic fragments of effective spherical radii

Downloaded from rsta.royalsocietypublishing.org

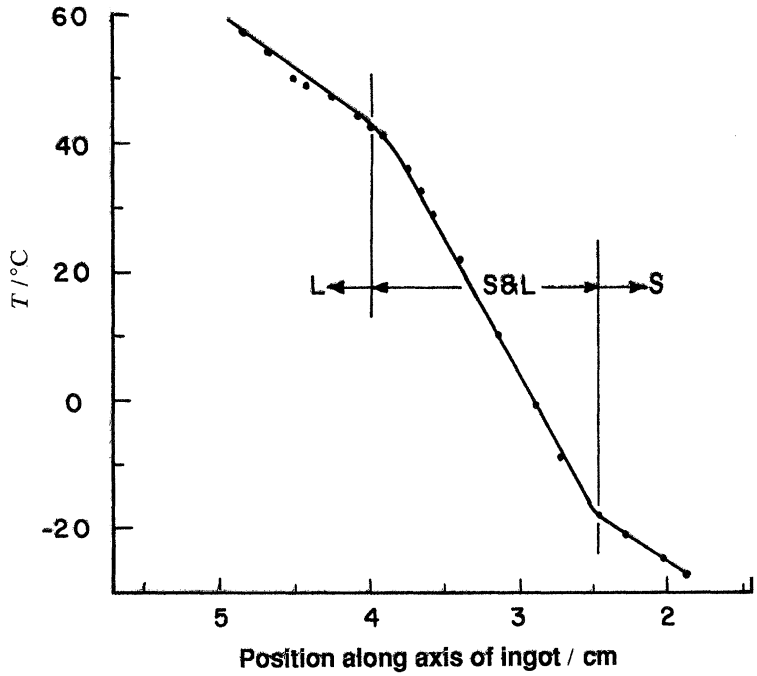

Figure 10. Vertical temperature profile in a NH_4Cl–68 wt% H_2O casting, 30 min after pouring, from open liquid, L, through the mush region, S and L, to the fully solid region, S; see figures 4 and 5.

ca. 20 μm to 100 μm. Although solid NH_4Cl is significantly more dense (*ca.* 35%) than the fluid, the fraction of solid within an imaginary spherical envelope is small so that the tendency to sink, as according to Stokes' law, is very small (Jang & Hellawell 1991) and the particles can be regarded effectively as of isodensity. In addition, by diffusing the light from the point source with a translucent sheet, it was possible to introduce a sharper, enhanced refractive index contrast, figures 9*a* and 23, which defined the plume compositional dimensions more sharply. It should be noted here, comparing figure 9*a*, *b*, that the range of the upward plume flow movements extends to at least twice that of the sharper composition profile; this is referred to in §6*b*.

A thermal record of the temperatures at different heights and times yielded temperature profiles of the type shown in figure 10. The lower inflection corresponds to the ice + NH_4Cl eutectic position and reflects the fact that the major phase, ice, has a thermal conductivity some four times that of the aqueous solution, being the major phase in the solid + liquid 'mushy' zone. As solidification proceeded and the bulk liquid cooled, the temperature gradient above the dendritic growth front decreased steadily from *ca.* 2.0 K mm^{-1} towards zero (Sample 1984).

Temperature differences, ΔT, were also recorded across convection plumes by moving a fine (0.076 mm), bare, chromel–alumel thermocouple horizontally through the visible plumes, close to and at various heights above the dendritic growth front. Figure 11 is an example of the type of temperature profile so detected.

Liquid compositions were measured during the present work using a Pulfrich type refractometer which measures the critical angle and provides the refractive indices to $\pm 2 \times 10^{-4}$, operating in a recirculating water bath at ambient temperatures up to

Downloaded from rsta.royalsocietypublishing.org

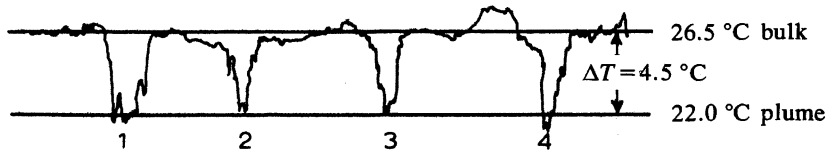

Figure 11. Showing temperature variations in NH_4Cl–70 wt% H_2O recorded by moving a fine, bare thermocouple through solute plumes close to (< 5 mm) the gradient front; $t = 40$ min.

65 ± 0.5 °C. With a solutal coefficient of *ca.* 2×10^{-3}, this allowed compositions to be expressed to within ± 0.1 wt%. With a thermal coefficient of 1.7×10^{-4}, any minor fluctuations in the ambient temperature were undetectable.

Liquid samples were taken directly using a micrometer syringe, driven by a servomotor to ensure a controlled rate of withdrawal of fluid. The arrangement is shown in figure 12. The syringe and drive were mounted on a Plexiglas sheet which was free to slide over a second sheet in which there was a large hole, so that it could therefore be positioned to locate individual plumes. The sampling needles were 150 mm long with a bore of 0.55 mm and outer diameter of 0.9 mm. With plume diameters around 1 mm, and with flow rates up to 8 mm s^{-1}, the sampling rate was kept below *ca.* 0.03 ml s^{-1} to avoid drawing up surrounding bulk liquid. Typically, the sampling rate was *ca.* 0.02 ml s^{-1}, so that excess plume liquid flowed up the sides of needles; samples up to 1 ml were taken in this way and were immediately ejected into small sealed vials before solid NH_4Cl could precipitate. Small drops of these liquid samples were placed in the refractometer and the indices were measured at a temperature above the relevant liquidus temperature, the instrument having been calibrated at that temperature using solutions of known composition. Plume and adjacent liquids were sampled within a few minutes; two needles were used and these and the syringe were washed, rinsed and dried between successive samplings. Up to ten pairs (plume and bulk) of samples were taken over times up to three hours from 'castings' having initial compositions of 68, 70 and 72 wt% NH_4Cl.

Plume sampling was necessarily restricted to not more than 20–30 mm above the growth front because (see later) plumes developed twisting, helical patterns at greater heights, so that it became impossible to take reliable samples. These helical patterns are described in more detail in Appendix C.

In addition to the above series of measurements on a given volume (500 ml) of poured solution, further experiments were carried out in which, after plume convection became well established ($\gtrsim 60$ min), the height of the upper meniscus was reduced by progressively siphoning off the supernatant bulk liquid. In these experiments, only flow rates and bulk liquid compositions were measured as functions of time and the height of the meniscus with respect to positions of the dendritic and eutectic fronts; see figure 15.

(*c*) *Organic systems:* SCN–EtOH

The nominal purity of commercially available SCN is not guaranteed at better than 99.0%, but there is a wide range of quality from batch to batch and the freshly prepared product is much clearer than older stock which degrades with time and becomes yellow. With relatively high concentrations of EtOH (up to 15 wt%), the base purity was not thought to be a critical issue, but the clear fresh stock was always used.

The experimental procedures for SCN base systems were essentially the same as for the aqueous systems previously described, with minor variations. Circular and

PHILOSOPHICAL TRANSACTIONS OF THE ROYAL SOCIETY A MATHEMATICAL, PHYSICAL & ENGINEERING SCIENCES

Downloaded from rsta.royalsocietypublishing.org

square section transparent moulds were of quartz or pyrex, rather than acrylic plastic with which SCN reacts. Solutions were poured from the same temperature, 80 °C, and composition ranges from 2.5 wt% EtOH to 20 wt% EtOH were examined, the majority of experiments being performed with the 15 wt% solution; see phase diagram, figure 7*d*.

The SCN based solutions differ from the aqueous systems in having smaller solutal coefficients of refractive index, i.e. NH_4Cl–H_2O, 1.8×10^{-3} against SCN–EtOH, 5.2×10^{-4}. As a result, the solute plumes are less easily seen by visual inspection and the angle of deviation for light refracted through the plumes is smaller by nearly one-third than in the aqueous case. Consequently, chemical analyses of plume and bulk liquids by their refractive indices were much less sensitive, and with an experimental latitude of $\pm 2 \times 10^{-4}$, compositions could not be specified more closely than *ca.* 0.4 wt%, which was almost within the range of the actual composition differences. Also, analyses in this system are complicated by the volatility of ethanol, producing further compositional uncertainties.

5. Results

A summary of measurements made on plume flow in the transparent systems, directly, and the corresponding posthumous data from lead alloys are summarized in table 2. This information is based on previously unpublished work (Sarazin 1990), supplemented by more recent measurements. The following comments and figures qualify the data in table 2.

(*a*) *Global*

(i) *Macroscopic dimensions*

Referring to the phase diagrams of figure 7*a–d*, the relative vertical heights within sample ingots after time of pouring into moulds are as shown in figure 13*a–c*, for representative compositions. It will be understood that the depth of the mushy zone varies with composition in each system according to the freezing ranges. As the figures show, the metallic samples solidify completely and in many cases the dendritic front reaches the upper meniscus before eutectic has started to grow through the mushy zone from the lower face. The transparent analogues, on the other hand, do not solidify completely unless the mould is sufficiently short. In all cases the mushy zones increase in depth with time.

In the lead alloys and in the SCN–EtOH system there is contraction during primary dendritic growth and at the eutectic/monotectic fronts, so that the upper meniscus falls continuously during an experiment. In the metallic sample the upper surfaces show dendrites in relief after interdendritic shrinkage has occurred. In the aqueous system there is contraction as the mushy zone forms, estimated to be *ca.* 5% (see Appendix A), but there is almost equivalent expansion with formation of the eutectic of which the major phase is ice. Initially, therefore, there is a small drop in the height of the meniscus, then the volume changes cancel out and the meniscus rises towards the original level.

(ii) *General plume characteristics in transparent materials*

Reference has already been made to a short-range finger zone, cf. §2. Plumes may form when the mushy zone has developed to a depth of $\gtrsim 5$ mm, typically after some 10–20 min, refer to figure 13*b*, *c*, and then replace the finger régime. Plumes evolve

PHILOSOPHICAL TRANSACTIONS OF THE ROYAL SOCIETY A MATHEMATICAL, PHYSICAL & ENGINEERING SCIENCES
PHILOSOPHICAL TRANSACTIONS OF THE ROYAL SOCIETY A MATHEMATICAL, PHYSICAL & ENGINEERING SCIENCES

Downloaded from rsta.royalsocietypublishing.org

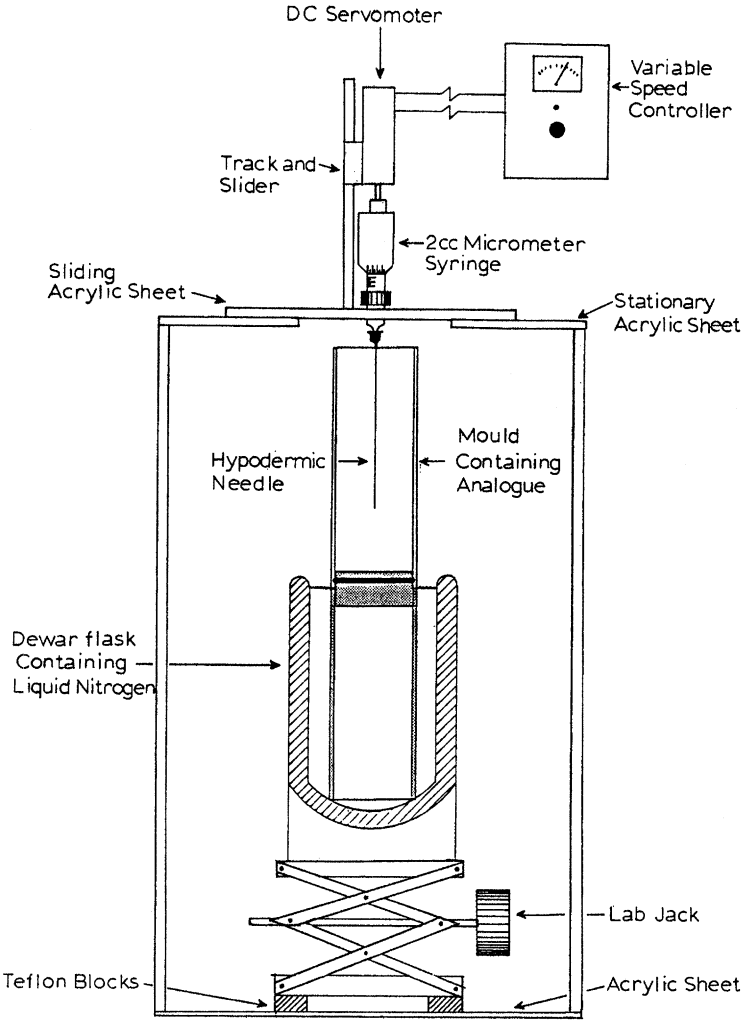

Figure 12. Diagram of experimental assembly used to extract plume and bulk liquid samples for chemical analysis.

Table 2. *Channel/plume data: summary of results (figure 5)*

	metallic (10 wt % Sn)	aqueous (70 wt % H_2O)	organic (15 wt % EtOH)
height, H_t (m)	?	> 0.1	~ 0.1
depth, D (m)	$> 5 \times 10^{-3}$	$> 5 \times 10^{-3}$	$> 5 \times 10^{-3}$
primary dendrite spacing, λ (m)	3×10^{-4}	$5\text{–}6 \times 10^{-4}$	$5\text{–}6 \times 10^{-4}$
radius, r (m)	$5\text{–}7 \times 10^{-4}$	$5\text{–}8 \times 10^{-4}$	$\sim 5 \times 10^{-4}$
spacing, L (m)	$\approx 5\text{–}10 \times 10^{-3}$	$5\text{–}10 \times 10^{-3}$	$5\text{–}10 \times 10^{-3}$
composition difference, ΔC (wt %)	1 to 3	1 to 2	$\gtrsim 1$
temperature difference, ΔT (K)	?	1 to 4	< 1
mean velocity, $\bar{v}$ (m s^{-1})	?	$6\text{–}9 \times 10^{-3}$	$\approx 1 \times 10^{-3}$

Downloaded from rsta.royalsocietypublishing.org

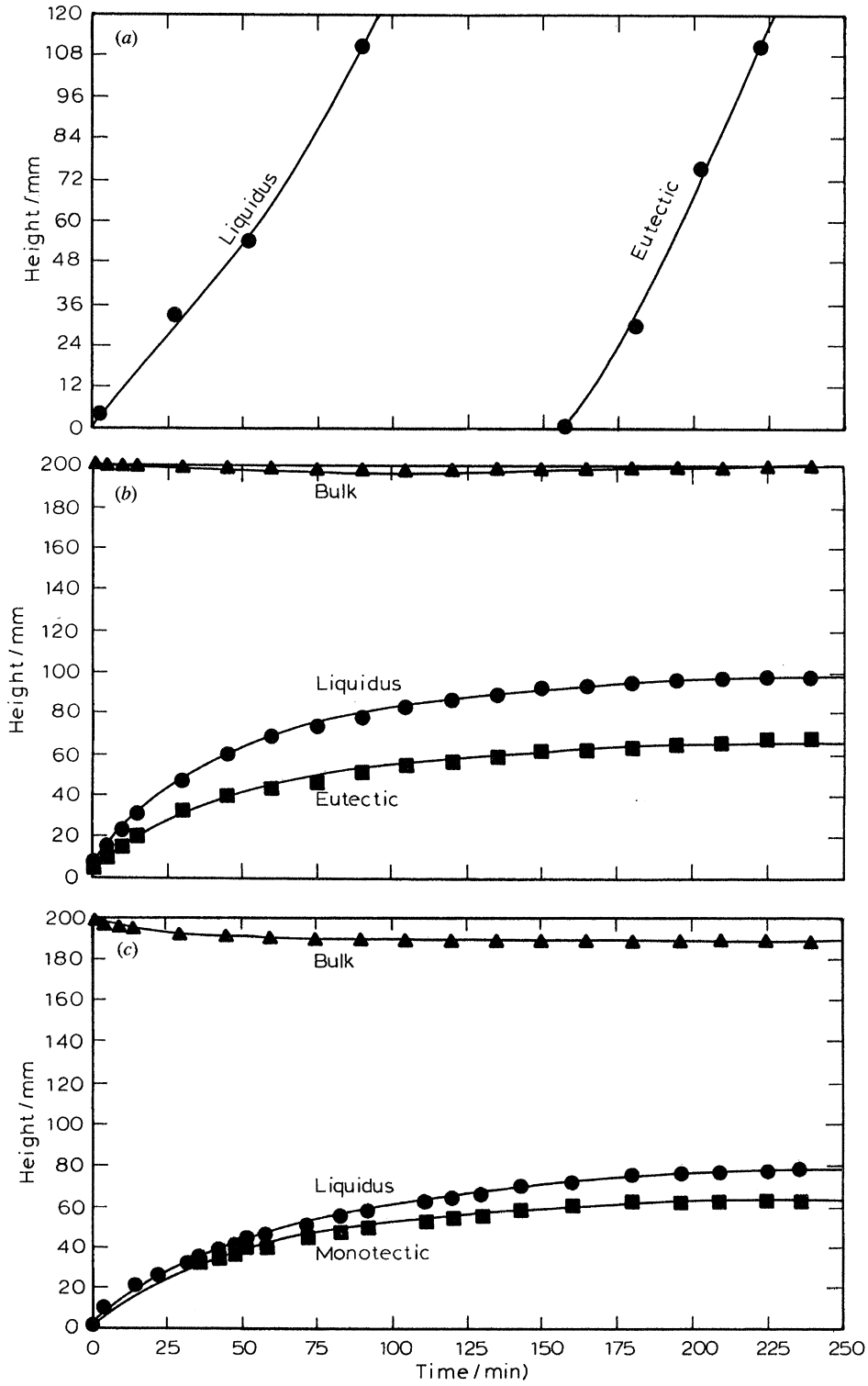

Downloaded from rsta.royalsocietypublishing.org

from levels close to the growth front and channels develop in the mushy zone beneath them, as depicted in figure 6. In the aqueous system these events happen rapidly, within *ca.* 20 s; in the organic system the perturbation is somewhat slower and may be recorded in some detail. As the perturbation develops, the dendritic front immediately beneath it shows a brief rise in level, which is rapidly followed by development of a channel and an upward surge or release of solute-rich liquid, which locally melts and sweeps out the concomitant channel (Hellawell 1987). Subsequently, within a few minutes, relatively rapid streamlined plumes are established, and these can extend to heights exceeding 200 mm in the aqueous system. In the aqueous system, plume flow is essentially straight and vertical for some 20–40 mm above the front, but then plumes gradually twist into a helical pattern of decreasing pitch, breaking into locally turbulent pockets near the upper meniscus and spreading out horizontally; see figure 4. Much later, after 2–3 h, solidification and plume activity decrease and stratified layers of different compositions may develop as has been previously reported (e.g. Chen *et al.* 1971; Huppert & Turner 1981; Sample & Hellawell 1982).

In the tall mould (1 m), the pattern is similar but attenuated somewhat to greater heights until plumes expand laterally and dissolve into locally turbulent 'clouds' or 'balloons' at heights *ca.* 250 mm above the growth front. On shadow graphs, faint signs of convection are perceptible at longer times up to heights of *ca.* 350 mm. In the short mould (0.1 m), plumes reach the upper meniscus without breaking down and spread out smoothly without apparent disturbance. In the standard mould (0.2 m), as turbulent pockets of solute-rich liquid impinge upon the meniscus, they cause visible ripples which can be viewed very clearly by reflection from beneath that surface.

In the organic system, where flow is more sluggish (e.g. 1 mm s^{-1}, see table 2), plumes do not show any tendency to adopt helical patterns but rise vertically until they broaden and begin to break down at *ca.* 100 mm above the growth front. The mode of breakdown follows a perturbation of the plume cylinders into expanding and dissolving globules of solute-richer fluid.

(*b*) *Microscopic dimensions*

(i) *Primary interdendritic spacings*, λ

This dimension depends, in a given system, upon the growth rate, V, temperature gradient, G, and liquid concentration, C_L, approximately with $V^{-\frac{1}{4}}$, $G^{-\frac{1}{2}}$, and $C_L^{\frac{1}{4}}$ (Kurz & Fisher 1986). It was not the object of the present work to follow the dependence of these spacings in a rigorous manner and, in any case, the design of the experiments does not lend itself well to that aim. Within the small ranges of these variables in the present work, the expected and observed effects are not large, and, in any case, primary dendrite spacings do not adjust rapidly to such changes as did occur; the coupling between adjacent dendrites is rather weak at low growth rates. The values given in table 2 may be regarded as typical for the prevailing conditions during active plume flow to within *ca.* $\pm 10\%$.

Figure 13. Positions versus time for dendritic and eutectic (or monotectic) growth fronts, including those of the upper meniscus in transparent systems; (*a*) Pb–10 wt% Sn; (*b*) NH_4Cl–70 wt% H_2O; (*c*) SCN–15 wt% EtOH. Refer also to the phase diagrams of figure 7*a*, *c*, *d*.

Downloaded from rsta.royalsocietypublishing.org

(ii) *Channel/plume radii, r*

In the metallic samples, channel widths were measured optically and simultaneously with composition profiles by EMPA. As explained, channels are not perfectly circular in section, cf. figure 8*b*, and radii are similarly difficult to define unambiguously. The range listed in table 2 is an average for a given alloy composition, but channels increase in width with alloy concentration and show a weak tendency to increase with height in a given sample (see Sarazin & Hellawell 1988). However, following a given channel through a succession of horizontal sections does not show any well-defined trend in width, nor, as will follow, any obvious correlation with solute concentration (see next section).

In the transparent materials, a distinction has already been made between composition profile and the velocity profile, and this will be discussed further. That which can be measured optically corresponds to the nearly square wave composition profile across a plume. The dimensions listed in table 2 relate to the lower levels of plumes before they adopt helical patterns or broaden at higher levels.

In general, channel or plume radii of metals and the transparent materials are remarkably similar and correspond to some two or three primary interdendritic spacings. This means that the plumes have cross-sectional areas which are about an order of magnitude greater than those of preceding fingers.

(iii) *Interchannel/plume spacings, L*

In general, the number of plumes and attendant channels in a sample decreases as the growth front rises (Sample & Hellawell 1984; Sarazin & Hellawell 1988). Figure 14 is taken from measurements on ten Pb–10 wt % Sn ingots as mean, near neighbour separations. While an average increase in L is evident, the distribution of channels is far from uniform and the scatter is large. What is remarkable, however, is that equivalent measurements over a range of compositions and from system to system (metallic, aqueous, organic) all fall within a similar broad band. The channel spacings were not less than an order of magnitude smaller than sample widths in the present experiments (e.g. *ca.* 5 mm against *ca.* 50 mm), so that wall effects are important and the measurements become very subjective. Interchannel interactions are clearly weak, but as a general observation, when two (or more) channels became closer than $\gtrsim 5$ mm, one of them would weaken and eventually die out, or, less frequently, two would combine to form a single channel (see Sarazin & Hellawell 1988, fig. 1).

For perspective, it is helpful to consider all these macroscopic and microscopic dimensions in terms of the primary interdendritic spacings, λ, so that on such a scale, $r \gtrsim 2\lambda$, $L \approx 20$–30λ, the plume heights, H_t, exceed 200–300λ.

(*c*) *Composition variations*

(i) *Bulk liquid or matrix*

The extent of fractional solute segregation upward along samples was measured from sections of the fully solidified metallic ingots (Sarazin & Hellawell 1988; Sarazin 1990) and directly by analysis of bulk liquid in the aqueous system, figures 15 and 16. Typically, the solute concentration rises in the shrinking volume of supernatant liquid by more than 5 %. Such segregation is only possible because there is convective transport of solute from the mushy zone up into the supernatant liquid. If plume convection is reduced, as by slow precessional or rocking movements

PHILOSOPHICAL TRANSACTIONS OF THE ROYAL SOCIETY A MATHEMATICAL, PHYSICAL & ENGINEERING SCIENCES

PHILOSOPHICAL TRANSACTIONS OF THE ROYAL SOCIETY A MATHEMATICAL, PHYSICAL & ENGINEERING SCIENCES

Downloaded from rsta.royalsocietypublishing.org

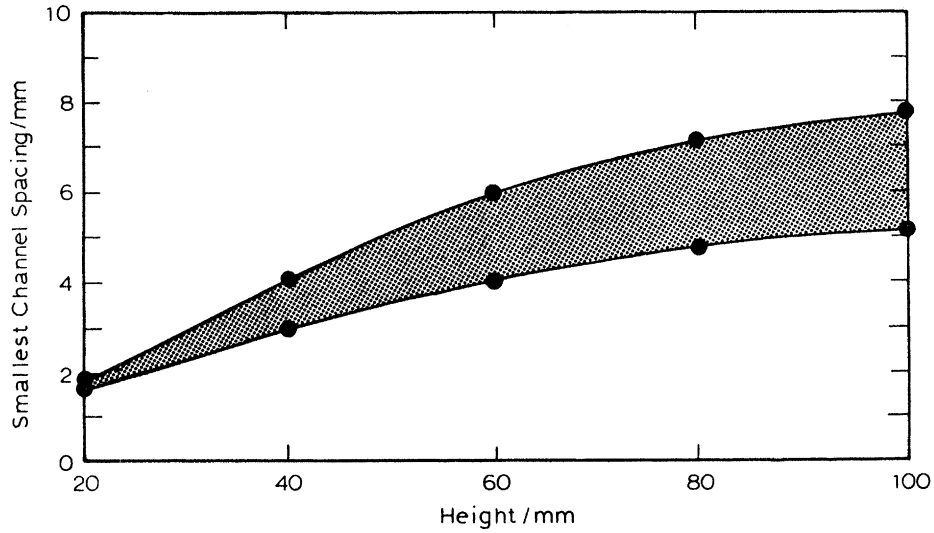

Figure 14. Range of interchannel spacings, L, as a function of height in a Pb–10 wt% Sn ingot.

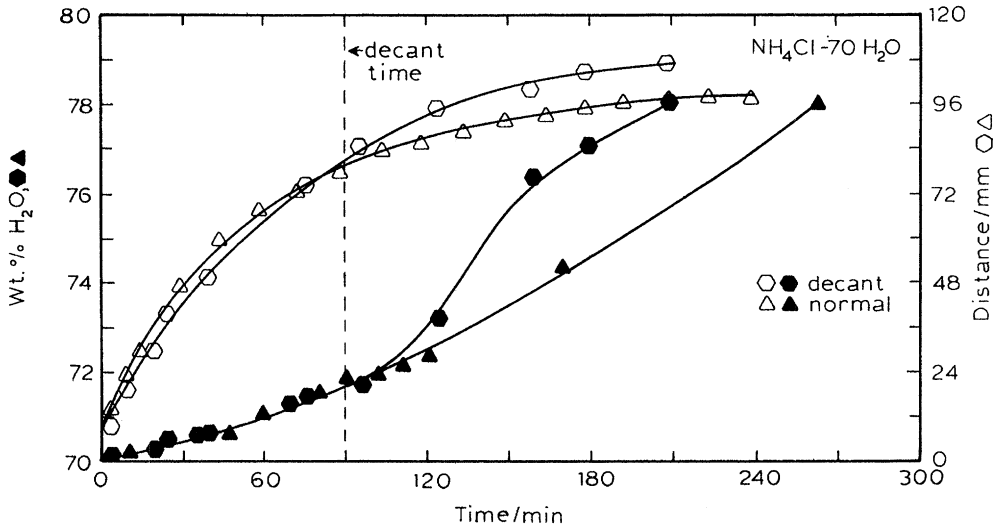

Figure 15. Bulk liquid analyses and positions of dendritic gradient front, versus time, for a normal casting, ▲, △, and one from which half of the supernatant liquid was decanted after 90 min, ●, ○, showing accentuated fractional segregation in the latter case.

(Sample & Hellawell 1982; Sarazin 1990), vertical macroscopic segregation is reduced because plume formation and convective transport are inhibited. With such macroscopic segregation, conservation of matter also requires that the volume fraction of dendritic solid in the mushy zone is higher than a simple lever rule proportion would suggest (Appendix A).

This macroscopic segregation can be accentuated if part of the supernatant liquid is decanted at some time after plumes and channels have become established. Figure 15 for the aqueous system includes this type of information for an uninterrupted experiment and one in which half the supernatant liquid was siphoned off after 90 min. Included on this figure are the heights of the dendritic growth front, which

PHILOSOPHICAL TRANSACTIONS OF THE ROYAL SOCIETY A MATHEMATICAL, PHYSICAL & ENGINEERING SCIENCES
PHILOSOPHICAL TRANSACTIONS OF THE ROYAL SOCIETY A MATHEMATICAL, PHYSICAL & ENGINEERING SCIENCES

Downloaded from rsta.royalsocietypublishing.org

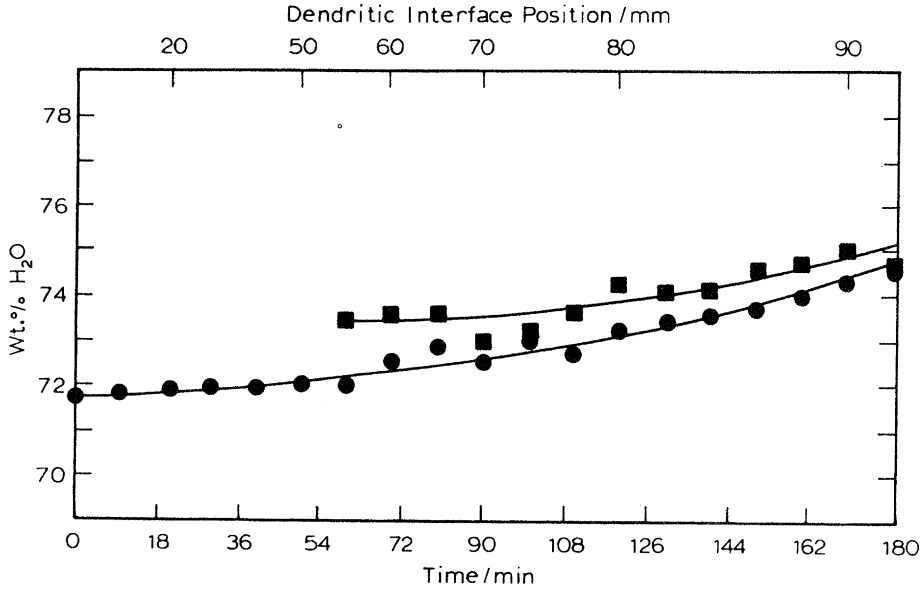

Figure 16. Analysed plume (■) and bulk (●) liquid compositions in a NH_4Cl–72 wt% H_2O casting as functions of time after pouring and of the position of the dendritic gradient front.

do not differ significantly, while the composition rises more rapidly in the reduced, smaller volume of supernatant liquid. As it happens, the plume flow rates also began to decrease in the decanted case because the plume-bulk composition difference, ΔC, also decreased and the buoyancy forces were correspondingly reduced.

(ii) *Channel and plume compositions*

It is important to reiterate here that analyses of channels in metallic samples are post mortem and those of plumes in the transparent systems are *in situ*; this is discussed later in §6*d*. These compositions were used to calculate buoyancy contributions and to analyse flow rates and were therefore critical in making extrapolations from one system to another.

In both lead–tin and lead–antimony alloys, compositions of the channels and of the surrounding matrices were examined in detail as functions of bulk initial concentrations, C_0, position along samples, and for individual channel radii, r (Sarazin 1990). There is a small rise in the concentration difference, ΔC, with C_0, e.g. from *ca.* 2 wt% in Pb–5 wt% Sn to *ca.* 3.5 wt% in Pb–15 wt% Sn, but no clear correlations with position, H_t, or with channel radius, r.

In the aqueous system, corresponding plume and bulk liquid compositions, C_L, were followed for three initial compositions, C_0, of 68 wt% H_2O, 70 wt% H_2O, and 72 wt% H_2O. Figures 16 and 17 are for the last of these and are typical, showing that as C_L rises by macroscopic segregation, the plume composition difference, ΔC, gradually decreases from about 1 wt% after one hour to *ca.* 0.5 wt% after 3 h. This decrease is not attributed to any dependence on the bulk concentration, *per se*, but rather to the phase change gradually becoming slower at longer times.

The aqueous measurements were, when possible, restricted to a single plume, whereas in the metallic samples many channels were examined in an ingot. As previously explained, cf. §4, the sensitivity of refractive index measurements in the

Downloaded from rsta.royalsocietypublishing.org

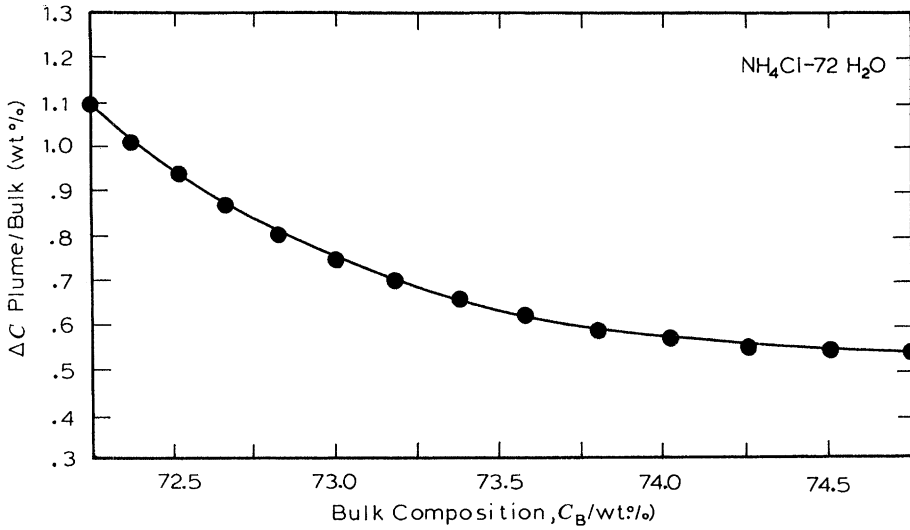

Figure 17. Plume versus bulk liquid composition difference, ΔC, plotted against bulk liquid composition, C_L. Data obtained by smoothing the data from figure 15.

organic system is such that the composition difference, ΔC, was barely significant compared with the margin of error which is involved, e.g. ± 0.4 wt% on a difference, $\Delta C \approx 1.0$ wt% EtOH.

(*d*) *Plume temperature differences*, ΔT

Meaningful measurements were limited to the aqueous system; those in the organic system were too small to be significant. No attempt to search for thermal plumes in the metallic samples was made.

As shown in figure 11, plume liquid flowing out of channel mouths was cooler than the surrounding bulk liquid by as much as 4 K, but as the plume liquid rose it rapidly approached the ambient temperature, so that ΔT typically fell to *ca.* 1 K at a height of 30–40 mm above the growth front, i.e. after a time interval of *ca.* 5 s.

With a temperature gradient in the mushy zone $\gtrsim 1$ K mm^{-1}, the value of ΔT of *ca.* 4 K for liquid flowing out of channel mouths suggests that it came from a level not deeper than *ca.* 4 mm below the level of the front. With a liquidus slope of *ca.* 5 K wt%$^{-1}$, this is also compatible with the observed composition difference, ΔC, of *ca.* 1 wt% H_2O. Re-entrainment of bulk liquid through the mushy zone is limited, therefore, only to the upper levels of that zone.

The fact that little or no temperature difference was detectable in the organic system may be attributed to the lower flow rates involved, while the thermal conductivities were similar; see tables 1 and 2.

(*e*) *Plume flow rates*, $\bar{v}$

The values listed in table 2 are velocities based upon a large number of particulate movements, cf. §4, and are taken as mean velocities, $\bar{v}$. A detailed assessment of the velocity profile has not yet been made.

In both transparent systems, flow rates are relatively slow and irregular as plumes begin to form, but accelerate over short periods (*ca.* 10 min) as plumes become established. The values quoted correspond to the established, quasi-steady state flow within *ca.* 5 mm of the gradient front at times less than one hour.

PHILOSOPHICAL TRANSACTIONS OF THE ROYAL SOCIETY A MATHEMATICAL, PHYSICAL & ENGINEERING SCIENCES
PHILOSOPHICAL TRANSACTIONS OF THE ROYAL SOCIETY A MATHEMATICAL, PHYSICAL & ENGINEERING SCIENCES

Downloaded from rsta.royalsocietypublishing.org

At longer times and at higher levels in the mould, flow rates noticeably fall as the growth of crystalline material ceases. These decreasing rates correspond to the rising solute concentration in the bulk liquid and decreasing composition differences between plume and bulk liquids, as shown in figures 16 and 17. The flow rates also fell with decanting experiments, figure 15, previously described, and these are again attributed to falling buoyancy contributions.

As already explained, it was difficult to measure flow rates in helical plumes with any precision, but it could be observed that the flow rate along a plume was more rapid than the climb of the helical patterns themselves, arising from their rotation. These more complex movements are discussed in Appendix C.

6. Discussion

(*a*) *Mass balance*

The convective behaviour which has been described is driven by a continuous phase change, and the system selects a mechanism and scale which balance the solidification rate. The continuous liquid mixing which is achieved by plume flow cannot be adequately described by considering the problem simply as a consequence of density inversion between two liquid layers of given initial compositions.

To illustrate the continuity of the process, a simple mass balance estimate confirms that the change in composition of the supernatant bulk liquid, C_L, matches the mass of solute ejected by plume flow, as indeed it should. For example, referring to the relative volumes and composition changes which occur in an aqueous casting, we have the following:

For an initial composition, C_0, of 70 wt% H_2O, the bulk liquid composition change, $\delta C = C_L - C_0$, is *ca.* 4 wt% H_2O over a period of *ca.* 170 min, similar to that shown in figures 15 or 16. The mass of water received per second into the supernatant liquid is then given by height, H_t, $\times$ mould cross section (1.87×10^{-3} m^2), $\times \delta C \times$ density, divided by time *ca.* 8×10^{-7} kg s^{-1}. This rate of solute supply is approximately the same as that estimated from the plume activity. Specifically, the mass of water ejected from an average of about 10 plumes, with radii *ca.* 5×10^{-4} m, mean flow rates *ca.* 10^{-2} m s^{-1}, and having composition differences, $\Delta C \approx$ 1 wt% H_2O, is then *ca.* 7.5×10^{-7} kg s^{-1}. Similar estimates apply to the metallic castings (Sarazin *et al.* 1988; Sarazin 1990).

At the same time, although the greater part of the bulk liquid is quiescent, it is actually recirculating slowly to balance the relatively small volume which is rising in the plumes. Again, taking the same mould cross section with about 10 plumes, each of cross section *ca.* 10^{-6} m^2, the upward flowing area is only *ca.* 0.5% of the total. With maximum plume flow rates of *ca.* 10^{-2} m s^{-1}, the necessary rate of downward flow in the bulk liquid is then *ca.* 5×10^{-5} m s^{-1}, taken across the entire cross section. In the organic system these estimates will be about an order of magnitude smaller, and in metals, at least an order of magnitude larger (see the analysis of plume flow rates in the following section).

As a general observation, it is worth mention that, although the bulk liquid appears clear to the naked eye, magnification reveals that there is a remarkably high density (e.g. 10–10^2 mm^{-3}) of small dendritic fragments carried up by plumes, which gradually sink back between them, figure 9*b*. This occurs despite the fact that there is a small, but finite, positive temperature gradient above the growth front. This observation is taken to further emphasize that grain nucleation in castings is in many

Downloaded from rsta.royalsocietypublishing.org

Table 3. *Some derived estimates for thermal and solutal transport, from tables 1 and 2*

	metallic (10 wt % Sn)	aqueous (70 wt % H_2O)	organic (15 wt % EtOH)
Péclet number, *Pe*			
(*a*) thermal, $\bar{v}r/\kappa$	13	23	5
(*b*) solutal, $\bar{v}r/D_L$	5×10^4 [a]	2.5×10^3	5×10^2
heights to reach equilibrium (m)			
(*a*) $H_T = \bar{v}t_T$	4×10^{-3} [a]	2×10^{-2}	2×10^{-3}
(*b*) $H_S = \bar{v}t_S$	13 [a]	2	2.5×10^{-1}
(*c*) observed	unknown	3×10^{-1}	1×10^{-1}
where $t_T = r^2/\kappa$ and $t_S = r^2/D_L$			

[a] Estimated.

cases almost automatically accomplished without recourse to mechanisms involving heterogeneous nucleation on identified or unidentified substrates (Jackson *et al.* 1966; Hunt 1984; Ohno 1987; Hellawell 1990). Quantitative description of how dendrites ripen and fragment, and how the resulting crystals are dispersed throughout the melt, is an essential part of any physically meaningful, predictive model of the overall solidification process during foundry operations.

(*b*) *Plume flow and analysis*

Disregarding the helical complications of flow in the aqueous system, to a first approximation plumes can be considered as vertical cylindrical tubes, increasing somewhat in diameter at the upper ends and effectively immersed in the permeable dendritic mesh at the bases. There is a loss of momentum at the top of plumes and some restriction at the bottom where liquid enters the tube. The entrainment concerns a limited volume of the mushy zone, not deeper than about half the separation between adjacent channel/plumes; measured plume liquid compositions and temperatures are consistent with this. In the plume tubes, thermal equilibrium with the bulk liquid is approached rapidly but solutal diffusion is much too slow for this to happen until later (higher levels). It is assumed here that the plume liquid leaving the channel exit has an approximately square wave composition profile, as the optical contrast indicates.

The available data in tables 1 and 2 may be used to express thermal and solutal Péclet numbers,

$$Pe_T = \bar{v}r/\kappa \quad \text{or} \quad Pe_S = \bar{v}r/D_L,$$

the former being around 10 but the latter being several orders of magnitude larger. These numbers then indicate that observed flow rates are a little too rapid to allow thermal equilibrium between plume and bulk fluids but are much too rapid for there to be any significant solute diffusion.

Alternatively, the times, t_T or t_S, needed for thermal and solutal diffusion might be estimated by equating plume radii, r, with $\sqrt{(\kappa t_T)}$ or $\sqrt{(D_L t_S)}$, and by taking observed (or estimated) flow rates, v, these then provide estimates of the heights at which such equilibrium might be achieved, $H_T = vt_T$ and $H_S = vt_S$, where κ and D_L are the diffusivities defined in table 1. These heights would be equivalent to those at which the fluids became isodensity by either diffusive process. As may be seen, table 3, the heights, H_T, to come to thermal equilibrium are small by comparison with observed plume heights, but those estimated for solutal equilibrium are actually

PHILOSOPHICAL TRANSACTIONS OF THE ROYAL SOCIETY A MATHEMATICAL, PHYSICAL & ENGINEERING SCIENCES
PHILOSOPHICAL TRANSACTIONS OF THE ROYAL SOCIETY A MATHEMATICAL, PHYSICAL & ENGINEERING SCIENCES

Downloaded from rsta.royalsocietypublishing.org

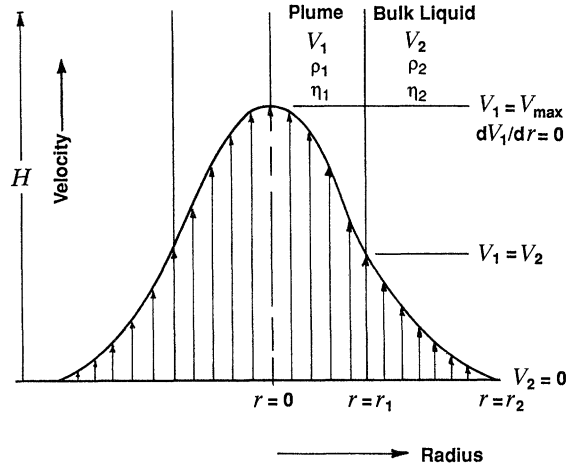

Figure 18. Schematic velocity profile through a plume of apparent (composition dependent) radius, $r = r_1$, out to some limiting radius, $r = r_2$. 'Internal' velocity, v_1, and 'external' velocity, v_2. See discussion, §*b*, and Appendix B.

larger than those observed in the transparent systems. This latter discrepancy may be understood if it is remembered that the flow rates are lower at greater heights as plumes become wider, develop into helical patterns and break down.

To make comparisons between the different systems, in particular to extrapolate from the transparent materials to metals, it is necessary to analyse the expected flow rates within and around solute plumes. To do this, it may first be assumed that within the plume, as defined by the sharp composition profile, r_1 of figure 18, the streamlined velocity will be described by Poiseuille flow. This gives a parabolic profile with a maximum, v_0, at $r = 0$,

$$v_0 = Pr_1^2/4h\eta,$$

where P is the buoyancy pressure difference and h is the plume height; here, $h = H_t$ (figure 5).

In the present context, $P = \Delta\rho \times g \times H_t$, where $\delta\rho = \rho(\beta\,\Delta C - \alpha\,\Delta T)$, so that

$$v_0 = \delta\rho\, g r_1^2/4\eta$$

and is independent of plume height. However, this would be equivalent to a 'no slip' condition at the plume walls and is not physically realistic, because the plume liquid is shearing through the bulk and dragging some of the surrounding liquid with it, to give an extended velocity profile, v_2, beyond $r = r_1$. The extended or outer velocity profile beyond r_1 may be described by a spline function to provide a modified Poiseuille expression (MP) to account for the fact that v_1 at $r = r_1$ must be finite.

In the present approach, see Appendix B, it has been assumed that the profile for v_2 is of exponential form. Such a velocity distribution allows for some expression of plume interactions if the profile for v_2, figure 18, is curtailed at some value of $r = r_2$, such as half the average interplume separation, L, in table 2 and figure 14. Beyond this distance, $r_2 = \frac{1}{2}L$, the bulk liquid automatically falls into the range of influence or 'watershed' for an adjacent plume. The expression for a maximum velocity at $r = 0$, assuming constant viscosity, plume temperature and composition (Appendix B) is then

$$v_{max} = (\Delta\rho\, g r_1^2/4\eta)\,[\ln r_1/r_2 - \tfrac{1}{2}].$$

PHILOSOPHICAL TRANSACTIONS OF THE ROYAL SOCIETY A MATHEMATICAL, PHYSICAL & ENGINEERING SCIENCES
PHILOSOPHICAL TRANSACTIONS OF THE ROYAL SOCIETY A MATHEMATICAL, PHYSICAL & ENGINEERING SCIENCES

Downloaded from rsta.royalsocietypublishing.org

Taking $r_2 = \frac{1}{2}L$ as having a typical value *ca.* 5 mm and substituting data from tables 1 and 2 then yields a very satisfactory result for $v_{max} = 7.5$ mm s^{-1}, compared with the experimental observations between 6 and 9 mm s^{-1}.

Again, considering the organic case, with the previous reservation about the significance of the plume composition measurements, the modified analysis would predict a maximum plume flow around 1.5 mm s^{-1}, which is only slightly higher than that observed (*ca.* 1 mm s^{-1}).

Finally, it is of interest to extrapolate the analysis to the metallic systems to find what flow velocities might be predicted. Taking a mean value of $\Delta C \approx 1.5$ wt% Sn (measured after the event) in a 10 wt% Sn alloy yields, with the same values of r_1 and r_2, a velocity maximum of *ca.* 140 mm s^{-1}. In Pb–Sb alloys the value would be a little lower, *ca.* 100 mm s^{-1}. This is a somewhat dramatic conclusion, implying that plumes rose through an experimental ingot in about 1 s. It is not incompatible with other estimates for thermally induced convection in metals, which are as high as 0.4 m s^{-1} (Gebhart *et al.* 1988).

It will be appreciated, in all of these estimates, that there is a scatter of at least ± 10% in the accepted plume radii and their compositions, and therefore a correspondingly larger range in the choice of velocity maxima. Nevertheless, considering the difficulties of precise measurement, the analysis provides good agreement with the optically observed flow rates at the base of plumes and lends some confidence to the prediction of the corresponding flow rates in metals. There remains, however, the physical limitation to the model, despite its apparent success in predicting the observed flow rates for the two transparent systems, in that it relates to a single plume and, although the value for r_2 is taken from typical interchannel/plume spacings, there is no account taken of the necessary but very slow downward flow which must occur to balance the overall circulation.

(*c*) *Selection of dimensions*

To better understand how a system selects channel/plume dimensions, plume compositions, buoyancy forces, and flow rates, we consider the expected variations of flow rates with plume radius for measured conditions. These can also be usefully compared with two limiting conditions for plume flow rates, namely that they must be sufficiently rapid at least to allow thermal equilibrium to be attained – a lower limit – but within a range which falls below that leading to turbulence, which must be an upper limiting condition. For the lower boundary it may be assumed that $v \approx \kappa/r$, and for the upper, $v = Re\,\nu/r$, where Re is the Reynolds number vr/ν. Then, in figure 19*a–c*, on logarithmic scales, are plotted velocities predicted from the foregoing analysis (MP (modified Poiseuille)) and the corresponding lower and upper limits, assuming a Reynolds number of 10^3 for the latter turbulence limit. Indicated on these graphs are the observed data for the aqueous and organic systems, covering small ranges of r and v, and a range of observed channel radii for Pb–10 wt% Sn, for which the MP analysis would predict a velocity range between *ca.* 100 and *ca.* 175 mm s^{-1}. One notes that the observed and predicted flow rates lie far below those for which the onset of turbulence would be expected, even in the metallic case, but also lie above the range for thermal equilibrium, by about one order of magnitude – as measurement has shown and the estimated Péclet numbers would imply.

From the preceding it appears that interplume separation is of minor importance and that the plume dimensional and compositional features are not selected by any obvious fluid flow limitations, although they are remarkably specific and closely

PHILOSOPHICAL TRANSACTIONS OF THE ROYAL SOCIETY A MATHEMATICAL, PHYSICAL & ENGINEERING SCIENCES
PHILOSOPHICAL TRANSACTIONS OF THE ROYAL SOCIETY A MATHEMATICAL, PHYSICAL & ENGINEERING SCIENCES

Downloaded from rsta.royalsocietypublishing.org

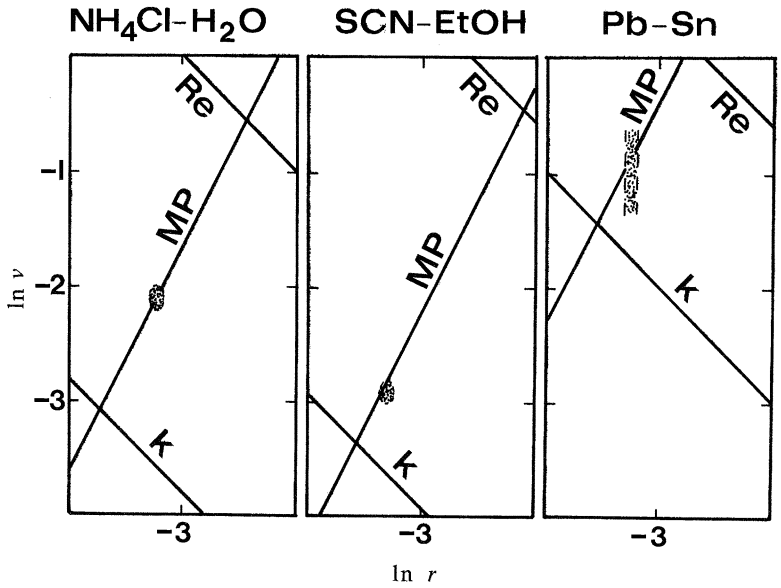

Figure 19. Logarithmic plots of plume flow rates, v, versus plume radii, r, for the aqueous, organic and metallic systems. The lines, MP, are predicted by a Modified Poiseuille analysis. The lines, *Re*, are for the onset of turbulence, $v = Re\,\nu/r$, with $Re = 10^3$. The lines, κ, correspond to $v = \kappa/r$, which would permit thermal equilibrium to be attained. The shaded regions indicate observed results for the transparent systems, and for the metallic systems show the observed range of radii for unknown velocities.

similar from system to system. Therefore, this leads to the conclusion that the selection of buoyancy contributions and plume dimensions (and therefore flow rates) is largely determined by the fluid entrainment restrictions which are imposed within the upper few millimetres of the dendritic mushy region.

Whether or not plumes develop from the boundary layer, by coupling between smaller fingers and bulk liquid, depends upon a wave length selection process, on the one hand, but, on the other, cannot be sustained if the upper part of the dendritic mesh is insufficiently permeable to allow the necessary entrainment to sustain such a large perturbation.

(*d*) *Entrainment and channel structure*

It is difficult to do justice to the observed dynamic fluid movements with only single frame exposures, e.g. figure 9*a*, *b*. However, it is clear from the foregoing and from previous observations (Copley *et al.* 1970; Sample & Hellawell 1982, 1984) that plume flow is sustained by re-entrainment of supernatant liquid close to the mouth of channels and that liquid at depths greater than *ca.* 5 mm (or about half the interchannel spacing) below the growth front remains essentially stagnant within the mushy zone, once channel plumes are formed. As recirculated liquid is cooled within the mushy zone and flows out of channel mouths, a cone of dendrites builds up around the exit. This happens after some 10–20 min in the aqueous system, figures 4 and 9, can be detected in metallic sections (Sarazin 1990), but is barely detectable in the organic material where fluid flow is much slower and the plumes are much closer to thermal equilibrium with the surroundings. Once these porous cones are established, much of the re-entrainment actually takes place by a shorter circuit

Downloaded from rsta.royalsocietypublishing.org

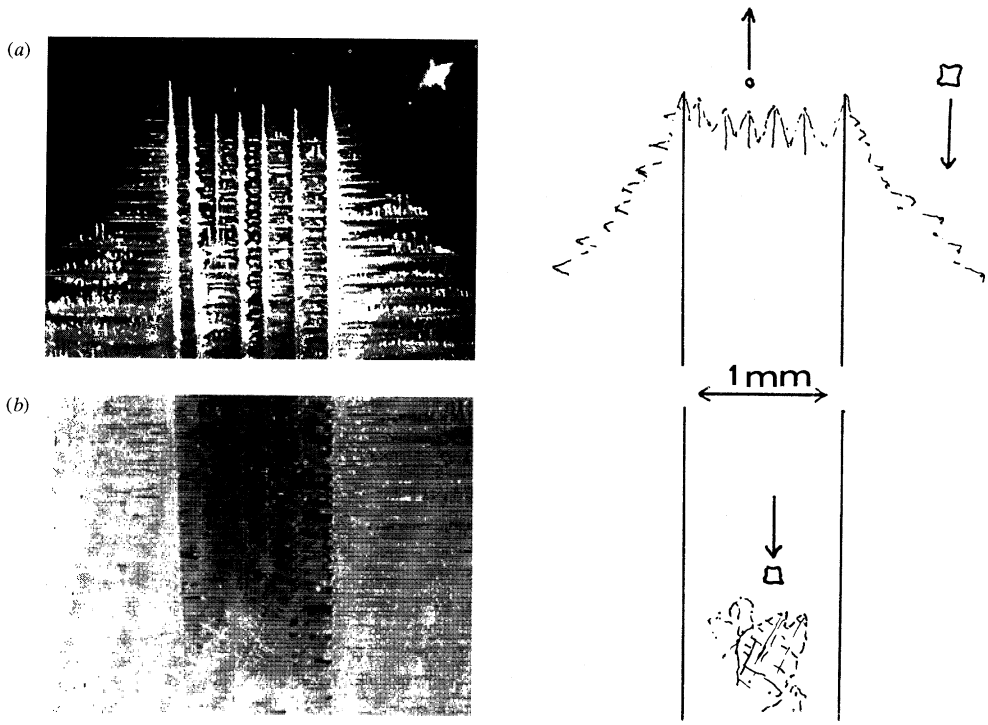

Figure 20. Taken from video frames of a channel in NH_4Cl–70 wt % H_2O which formed against the transparent mould wall, (*a*) at the mouth of the channel and (*b*) 8–10 mm lower in the mushy region. At the upper level (*a*), flow is upwards and a dendritic fragment is being ejected; in (*b*), the liquid is quiescent and a particle is sinking to accumulate as debris within the channel. Refer also to figure 1.

through them, leaving levels more than a few millimetres below the plane of the growth front quiescent.

The solid fraction in the upper levels of the mushy zone is small, typically around 10 % or less, so that the interdendritic liquid is continuous and the array is very permeable. Estimates of the interdendritic flow rates and scales thereof (Sample & Hellawell 1984) indicate a Reynolds number *ca.* 10, so that despite any tortuosity of the paths, flow is essentially streamlined. There are numerous approximations to flow of this type through porous media (D'Arcy 1856; Mehrabian *et al.* 1970; Geiger & Poirier 1973; Meyer & Smith 1985), but they do not extend to high liquid (or gaseous) fractions. At low liquid fractions the flow can be described as taking place along tubes within a solid matrix, but as the liquid fraction increases (perhaps beyond *ca.* 0.65), there is a transition or discontinuity in the type of flow involved to one occurring around rather than through the solid array (Ganesan & Poirier 1990; Ni & Beckermann 1991). This is a complex problem, depending also on the orientation of the solid obstacles (i.e. dendrites) and is beyond the scope of this paper, important though it is.

The structure within fully solidified channels deserves some comment since it also relates to the depth to which plume and channel activity are coupled within the mushy zone. As shown in figure 8*a*, segregation channels are clearly distinguished, microscopically, as regions containing more of the duplex eutectic than elsewhere, but they are by no means entirely eutectic, as they would be if that front had simply

Downloaded from rsta.royalsocietypublishing.org

grown through an open cylindrical channel within the dendritic array. At the same time, it is apparent, figure 20*a*, *b*, that at the mouths of channels and down into the mushy zone for nearly 10 mm, a channel is essentially an open cylinder. However, further down the channels, where the liquid is quiescent, dendritic crystal fragments from the channel walls are not ejected upwards, but sink and collect as polycrystalline debris, eventually to be surrounded by a smaller fraction of the eutectic structure. The polycrystalline structure of such superficial channels is clearly shown by deep etching of the surfaces of ingots, figure 1*a*, *b*, and may be understood with reference to figure 20.

These observations have particular relevance to the extrapolation made here from plume flow rates in the transparent systems to what might be expected in metals, using buoyancy estimates in the latter which were based on post mortem composition data. Although the plume and channel composition differences, ΔC, are similar (actually about twice as high in the metallic samples), the direct measurements relate to the immediate consequences of fluid recirculation near channel mouths and the posthumous data to quiescent channels of liquid which became blocked by debris at later times. For this reason we are inclined to regard the estimates of flow rates in metallic plumes, by extrapolation, as probably being too high by a factor of about two. This uncertainty emphasizes the need in general studies of fluid mechanics to develop an experimental method for observation of fluid movements in opaque materials.

7. Summary and conclusions

1. Channel segregation has been examined after and during solidification in metallic, aqueous, and organic systems which cover a wide range of Prandtl numbers from *ca.* 2×10^{-2} to 20. Observations and analysis relate to a configuration where solidification proceeds vertically upwards into a positive temperature gradient and concerns composition ranges for which there is a significant, dendritic, solid–liquid 'mushy' zone. Channels of solute-rich material within a mushy zone form as a result of liquid perturbations in the vicinity of a dendritic growth front when a plume of solute-rich liquid, rising above that front, is sustained by entrainment of supernatant liquid. It is a minimum requirement that, for this to happen, the positive solutal density gradient below the growth front exceed the thermally stabilizing, negative density gradient above.

2. Plume flow rates were measured in the transparent aqueous and organic materials and were analysed by reference to direct measurements of plume dimensions, composition, and temperatures, using a modified expression for streamlined flow which accommodated for slip at plume walls. The same analysis was used with posthumous data obtained from solid, metallic alloy samples, to estimate the probable flow rates in the latter.

The measured flow rates for the more viscous organic material were *ca.* 1 mm s^{-1}; those in the aqueous solutions, *ca.* 10 mm s^{-1}; and those estimated for metals were between 100 and 200 mm s^{-1}. Reservations were noted concerning the validity of the extrapolation of the analysis based upon posthumous channel compositions, obtained from fully solidified metallic samples. The estimate for metallic flow rates was thought to be too high by a factor of about two.

3. The dimensions of plumes and channels in all three materials were remarkably similar. The observed and estimated flow rates were somewhat faster than would allow plume liquid to be at thermal equilibrium with surroundings, but were very

PHILOSOPHICAL TRANSACTIONS OF THE ROYAL SOCIETY A MATHEMATICAL, PHYSICAL & ENGINEERING SCIENCES
PHILOSOPHICAL TRANSACTIONS OF THE ROYAL SOCIETY A MATHEMATICAL, PHYSICAL & ENGINEERING SCIENCES

Downloaded from rsta.royalsocietypublishing.org

much slower than would be expected for breakdown of streamlined to turbulent flow. It was concluded that the liquid fraction and permeability of the upper part of the mushy zone is critical in allowing the entrainment necessary to sustain channel, plume convection. It is concluded that to be able to predict when channel convection will occur, it will be necessary to model the coupling of a perturbation within a preceding, short-range finger zone, with quiescent bulk liquid above, and with quiescent interdendritic liquid immediately below the plane of the growth front.

4. Direct observation, and composition and temperature measurements in the aqueous system show that the fluid flow which sustains quasi-steady state plumes is limited to the upper *ca.* 5 mm of a mushy zone, and below that level the interdendritic and channel liquid is essentially quiescent. Dendritic fragments from channel walls in the upper regions are swept upwards with the plume liquid, while those detached from channel walls in the quiescent regions sink to a lower level and accumulate as polycrystalline debris. This is the origin of the equiaxed grain structure which is found in channels or freckles of steel or superalloy castings.

5. Simple mass balance estimates from fluid flow have been included to confirm general macroscopic segregation effects and some observations are made concerning helical convection patterns which were observed in the aqueous system (Appendix C), although these are not thought to influence the formation or propagation of channels.

This work was carried out with the support of the National Science Foundation, Division of Materials Research, Grant no. DMR-88-10549, and the National Aeronautics and Space Administration, Department of Microgravity Science and Applications, through NASA Lewis Research Center, Grant no. NAG-3-560. Helpful discussions with colleagues, both within Michigan Technological University and elsewhere, are gratefully acknowledged.

Appendix A. Mass balance and the fraction of NH_4Cl solid in the mushy zone

It is relevant to consider the overall mass balance within the experimental system. If there were no convective mixing of bulk supernatant liquid during solidification, since there is no solid solubility of H_2O in NH_4Cl, the fraction of dendritic solid in the mushy region would be given by the lever rule. Thus a solution of composition $C_0 = 30$ wt% NH_4Cl would, at the eutectic temperature ($-16\,^{\circ}C$), with composition $C_{Eu} = 20$ wt% NH_4Cl, contain a fraction of solid, $\chi = 0.125$ by weight; i.e. $C_0 = 100\chi + 20(1-\chi)$, or, with the solid density about 1.5 times that of the liquid, a volume fraction *ca.* 8.7%.

However, as there is convective mixing in the liquid, there is fractional segregation up the sample, as analyses have shown, and the fraction of dendritic solid is somewhat higher. This fraction may be estimated from a simple mass conservation argument. Referring to figure 5 for a partly solidified sample of total height H_0 and initial liquid concentration C_0 wt% NH_4Cl:

For unit cross section, the total weight of $NH_4Cl = C_0 H_0$; after a time, t, the amount of salt remaining in the bulk liquid, concentration C_L, is given by $C_L H_t$, and the amount of NH_4Cl below the dendritic front is therefore $C_0 H_0 - C_L H_t$. Below the dendritic growth front is the mushy zone of depth D, and the fully solid region of dendrites plus eutectic of height H_S.

It will be assumed that the mean weight fraction of solid in the mushy zone is $\frac{1}{2}\chi$, where χ is that fraction at the eutectic temperature, and that the mean composition

Downloaded from rsta.royalsocietypublishing.org

of the interdendritic liquid, C'_{L}, is midway between that of the bulk liquid, C_{L}, and the eutectic, C_{Eu}; i.e. $C'_{\mathrm{L}} = \frac{1}{2}(C_{\mathrm{L}} + C_{\mathrm{Eu}})$. These approximations are allowable since the volume fraction of solid is relatively small and the liquidus slope is almost constant.

Mass balance then gives

$$H_0 C_0 - H_t C_{\mathrm{L}} = H_{\mathrm{S}}[100\chi + C_{\mathrm{Eu}}(1-\chi)] + D[50\chi + C'_{\mathrm{L}}(1-\tfrac{1}{2}\chi)].$$

Referring to figures 13*b* and 15, at a time of *ca.* 175 min:

$$H_0 = 200\ \mathrm{mm}, \quad H_t = 110\ \mathrm{mm}, \quad D = 30\ \mathrm{mm}, \quad H_{\mathrm{S}} = 60\ \mathrm{mm},$$

$$C_0 = 30\ \mathrm{wt\%\ NH_4Cl}, \quad C_{\mathrm{L}} = 26\ \mathrm{wt\%\ NH_4Cl}, \quad C'_{\mathrm{L}} = 23\ \mathrm{wt\%\ NH_4Cl},$$

or

$$200 \cdot 30 - 110 \cdot 26 = 60[100\chi + 20(1-\chi)] + 30[50\chi + 23(1-\tfrac{1}{2}\chi)]$$

and $\chi = 0.21$ (weight fraction), or $f_{\mathrm{S}} = 0.15$ (by volume), which is nearly double that expected from the phase diagram and lever rule. The same derivation, assuming the same dimensions but without macroscopic segregation, i.e. $C_{\mathrm{L}} = C_0$, yields the same result as the lever rule.

Appendix B. Plume flow with boundary movement

The following relates to figure 18 and the discussion, §6*b*, concerning the fact that a plume wall cannot be regarded as a rigid interface but is a region where a buoyant plume shears through the surrounding bulk liquid and drags some of it upwards.

For the interior of a plume, a parabolic velocity profile, v_1, is assumed to make a spline function with an external profile, v_2, of exponential form. The system is regarded as isothermal and the composition profile is uniform along the upward direction. The dynamic viscosities within/without the plume are η_1 and η_2.

Since the velocity is continuous, it follows that $v_1 = v_2$ at r_1, and the shear stresses are equal $\tau_1 = \tau_2$, and also that $\mathrm{d}v_1/\mathrm{d}r = \mathrm{d}v_2/\mathrm{d}r$ at the boundary.

The velocity in the plume, v_1, follows from a momentum balance,

$$v_1 = \Delta\rho\, g r^2/4\eta_1 + C_1, \tag{B 1}$$

where C_1 is a constant.

In the bulk liquid only viscous shear terms apply and $(\mathrm{d}/\mathrm{d}r)(r\tau_2) = 0$, so that from Newton's law,

$$\frac{\mathrm{d}}{\mathrm{d}r}\left(r\eta_2 \frac{\mathrm{d}v_2}{\mathrm{d}r}\right) = 0. \tag{B 2}$$

By integration with $v_2 = 0$ at $r = r_2$, we then obtain outside the plume:

$$v_2 = (C_2 \ln r - C_2 \ln r_2)/\eta_2, \tag{B 3}$$

where C_2 is a constant.

Since $v_1 = v_2$ at $r = r_1$, equating equations (B 1) and (B 3) yields

$$\frac{\Delta\rho\, g r_1^2}{4\eta_1} + C_1 = \frac{C_2}{\eta_2} \ln\left(\frac{r_1}{r_2}\right). \tag{B 4}$$

Rearrangement and solving for $\mathrm{d}v_1/\mathrm{d}r$ at $r = r_1$ then yields the constants C_1 and C_2, and

$$v_1 = \frac{\Delta\rho\, g r^2}{4\eta_1} + \frac{\Delta\rho\, g r_1^2}{2\eta_2}\left[\ln\frac{r_1}{r_2} - \frac{\eta_2}{2\eta_1}\right], \tag{B 5}$$

Downloaded from rsta.royalsocietypublishing.org

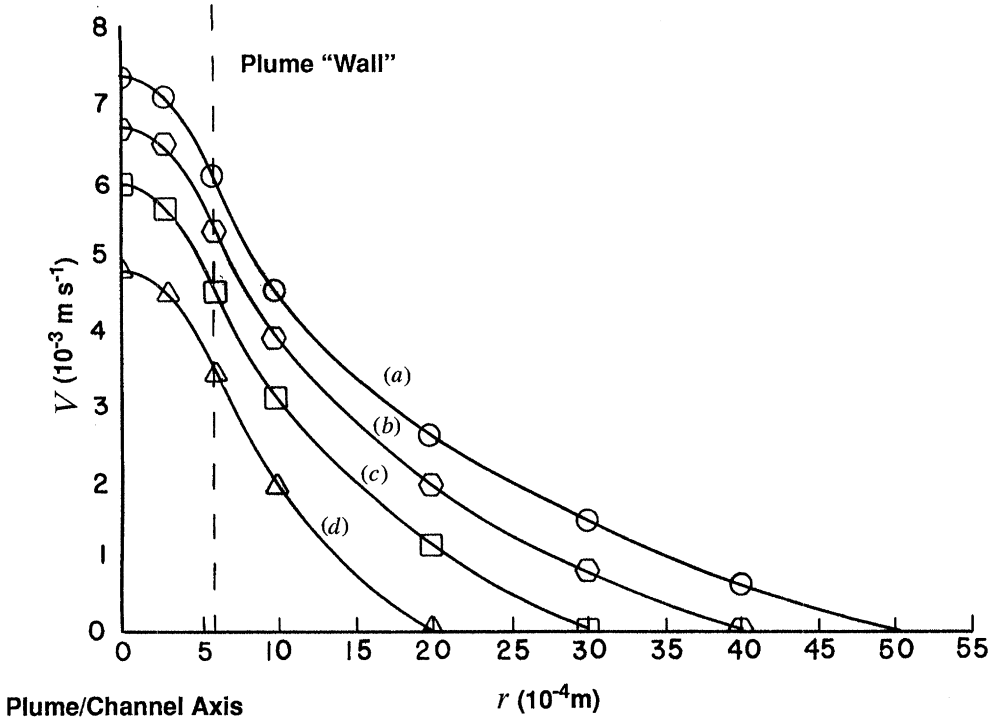

Figure 21. (*a*) $r_2 = 5 \times 10^{-3}$, (*b*) $r_2 = 4 \times 10^{-3}$, (*c*) $r_2 = 3 \times 10^{-3}$, (*d*) $r_2 = 2 \times 10^{-3}$.

or, with $\eta_1 = \eta_2$, $v_{\max}$ at $r = 0$ is given by

$$v_{\max} = \frac{\Delta\rho g r^2}{4\eta_1}\left[\ln\frac{r_1}{r_2} - \frac{1}{2}\right]. \tag{B 6}$$

This is the modified Poiseuille equation plotted for the various systems in figure 19.

The effect of curtailing the value of r_2, or reducing the ratio r_1/r_2 in equation (6), is shown in figure 21 for a decreasing range, $r_1/r_2 = \frac{1}{10}$ to $r_1/r_2 = \frac{1}{4}$. This comparison gives some feeling for the magnitude of plume interactions upon their separate flow rates.

We thank R. Kolkka of the Department of Mathematical Sciences at MTU for assistance with this derivation.

Appendix C. Helical plumes

As solute plumes twist into the helical mode, they do so in a left or right-handed sense. That this is so may not be obvious by inspection from the side, but can be more clearly seen by observation from above or at an oblique angle. As this pattern develops, the helices themselves rotate about their axes in a clockwise or anticlockwise sense, opposite to that of flow along the plumes. The helical pitch decreases with height until flow in the plumes begins to break out as locally turbulent 'snags' along the thread, and these briefly precede complete breakdown into locally turbulent 'clouds'.

Some helix dimensions and rotation rates are listed in table 4. It should be appreciated that these numbers can be only approximate, because the pitch of a

Downloaded from rsta.royalsocietypublishing.org

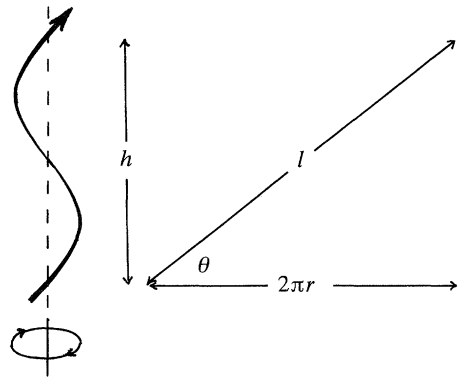

Figure 22. Schematic of plume-helix with dimensions listed in table 4.

Table 4. *Plume-helix dimensions*

	lower level	upper level
pitch height, h (mm)	18	22
radius, R (mm)	0.9	3.2
rotation period, τ (s)	6.5	15
θ	72.6°	47.7°
pitch $-\tan\theta = h/2\pi R$	3.18	1.1
plume length, l (mm)	18.9	29.7

given helix changes continuously with height. Referring to the schematic diagram, figure 22, and table 4, the relevant dimensions are the helix radius, R; the vertical height, h, for each turn of the thread ($2\pi R$); the length of the thread, l, for one turn; and the angular rotation period, τ, obtained from the distance, h, and the time taken for the pitch to rise over this distance. The data are from the lower level of a plume where the helical pattern begins ($H_t \approx 60$–80 mm), to an upper level where the helices broaden prior to breakdown of the plumes ($H_t \approx 120$–150 mm).

At a given height, an element of plume liquid of mass m is flowing upwards around a helix with a kinetic energy $\frac{1}{2}\, m\bar{v}^2$, while there is an angular kinetic energy of rotation, $\frac{1}{2}m\,(2\pi R\omega)^2$, where $\omega = 1/\tau$. We attribute the second contribution to the friction between the plume and bulk liquids, caused by viscous drag, so that the energy dissipated in this manner drives the rotation of the helix 'backwards' according to the sense of flow (i.e. right/left handed). It is instructive to calculate an intra-plume velocity at which an isodensity particle would appear to remain at a constant angular position in a helix. This would be a critical velocity, v_c, where the fluid in a plume was just able to 'keep up' with the helical counter-rotation, or, in effect, when the translational kinetic energy in the plume equals the angular kinetic energy of the helix itself. Values from the data in table 4 then yield $v_c = 3$ mm s^{-1} for the narrower, lower region of a helix, and $v_c = 2$ mm s^{-1} for the wider, more slowly revolving upper region. By comparison, actual flow rates in the plumes exceed these 'stationary' velocities by a factor of about two, so that only a proportion of the total kinetic energy is rotational. It is, of course, impossible that the intra-plume flow be slower than the critical rate, because that would imply that the fluid would sink, rather than rise in the helix.

These helical developments, at levels remote from the growth front, do not influence the propagation of channels within the mushy zone, which remain straight and perpendicular. They are of some interest in the present studies, however,

Downloaded from rsta.royalsocietypublishing.org

Figure 23. Synchronized helical flow in adjacent plumes, 'light field'. NH_4Cl–70 wt% H_2O, at a mean height of *ca.* 70 mm above growth front after 60 min.

inasmuch as the helical movements of adjacent plumes are often synchronized, figure 23, which is taken to reflect their weak, second-order interaction, cf. Appendix B.

The parallel may be drawn between these helical patterns and those of smoke plumes rising into still air. We suppose that they develop because they allow a more efficient displacement of the surrounding fluid, with downward, axial flow within the helix. We surmise that similar patterns would have developed in the more viscous organic system at longer times and greater heights, had the plumes not broken down by an alternative mechanism. There is presently no way of knowing if such helical flow occurs in metals because, as previously noted, their development is not reflected in the channel propagation.

References

Benon, W. D. & Incropera, F. P. 1987 *J. Heat Mass Transfer* **30**, 2161–2170.

Bridge, M. R., Stephenson, M. P. & Beech, J. 1982 *Metals Technol.* **9**, 429–433.

Chen, C. F., Briggs, D. G. & Wirtz, R. A. 1971 *J. Heat Mass Transfer* **14**, 57–65.

Chen, F. & Chen, C. F. 1988 *J. Heat Transfer* **110**, 403–409.

Copley, S. M., Giamei, A. F., Johnson, S. M. & Hornbecker, M. F. 1970 *Metallurg. Trans.* A **1**, 2193–2204.

Coriell, S. R., Cordes, M. R., Boettinger, W. J. & Sekerka, R. F. 1980 *J. Crystal Growth* **49**, 13.

D'Arcy, H. 1856 *Les fontaines publiques de la ville de Dijon*, pp. 376–382. Paris: Dalmont.

Fang, D. & Hellawell, A. 1988 *J. Crystal Growth* **92**, 364–370.

Felicelli, S. D., Heinrich, J. C. & Poirier, D. R. 1991 *Metallurg. Trans.* B **22**, 847–859.

Fisher, K. M. & Hunt, J. D. 1977 In *Int. Conf. on Solidification and Casting, Sheffield*, pp. 325–330, Book no. 193. London: The Metals Society.

Ganesan, S. & Poirier, D. R. 1990 *Metallurg. Trans.* B **21**, 173.

Gebhart, B., Jaluria, Y., Mahajan, R. L. & Samakia, B. 1988 *Buoyancy induced flows and transport*, ch. 1 and 4. New York: Harper and Row (Hemisphere).

Geiger, G. H. & Poirier, D. R. 1973 *Transport phenomena in metallurgy*, ch. 3. Addison-Wesley.

Grugel, R. N. & Hellawell, A. 1983 *Mater. Res. Soc. Proc.* **19**, 417–422.

Grugel, R. N., Lograsso, T. A. & Hellawell, A. 1984 *Metallurg. Trans.* A **15**, 1003–1011.

Hellawell, A. 1987 In *Structure and dynamics of partially solidified systems*, NATO Series E, vol. 125 (ed. D. E. Loper), pp. 3–22. Dordrecht: Martinus Nijhoff.

Downloaded from rsta.royalsocietypublishing.org

Hellawell, A. 1990 In *Proc. of F. Weinberg Intl Symp. on Solidification Processing* (Metallurgical Soc. Canadian Inst. Mining and Metallurgy), vol. 20, pp. 395–411 (ed. J. E. Lait & I. V. Samarasekera). Pergamon Press.

Holyer, J. 1981 *J. Fluid Mech.* **110**, 195.

Holyer, J. 1983 *J. Fluid Mech.* **137**, 347.

Holyer, J. 1984 *J. Fluid Mech.* **147**, 169.

Howard, L. N. & Veronis, G. 1987 *J. Fluid Mech.* **183**, 1–23.

Hunt, J. D. 1984 *J. Mater. Sci. Engng* **65**, 75–100.

Huppert, H. E. & Turner, J. S. 1980 *J. Fluid Mech.* **100**, 367–384.

Huppert, H. E. & Turner, J. S. 1981 *J. Fluid Mech.* **106**, 299–329.

Hurle, D. T. J., Jakeman, E. & Wheeler, A. A. 1982 *J. Crystal Growth* **58**, 163.

Jackson, K. A., Hunt, J. D., Uhlmann, D. R. & Seward, T. P. 1966 *Trans. Met. Soc. AIME* **236**, 149–158.

Jang, J. & Hellawell, A. 1991 *J. Ironmaking Steelmaking* **18**, 267–274 and 275–283.

Kaukler, W. F. & Frazier, D. O. 1985 *J. Crystal Growth* **71**, 340–345.

Kawamuri, T., Asai, S. & Muchi, I. 1988 *Tetsu-Tu-Hagane* **74**, 104–111,

Kurz, W. & Fisher, D. J. 1986 *Fundamentals of solidification*, pp. 240 and ch. 4. Switzerland: Trans. Tech. Publications.

Levin, E. M., Robbins, C. R. & McMurdie, H. F. 1964 *Phase diagrams for ceramicists and supplements I–V* (1970–1987). American Ceramic Society.

Mehrabian, R., Keane, M. & Flemings, M. C. 1970 *Metallurg. Trans.* A **1**, 1209 and 3238.

McDonald, R. J. & Hunt, J. D. 1969 *Trans. TMS-AIME* **245**, 1993–1996.

McDonald, R. J. & Hunt, J. D. 1970 *Metallurg. Trans.* A **1**, 1787–1788.

Meyer, B. A. & Smith, D. W. 1985 *Industrial and chemical fundamentals* **24**, 360–368. New York: American Chemical Society.

Moore, J. J. & Shah, N. A. 1986 *Int. metallurg. Rev.* **28** (6).

Ni, J. & Beckermann, C. 1991 *Metallurg. Trans.* B **22**, 349.

Ohno, A. 1987 *Solidification: the separation theory and its practical applications*. Springer-Verlag.

Pagalthivorthi, K. & Desai, P. V. 1986 In *Modelling of casting and welding processes* (ed. Kou & Mehrabian), pp. 121–132. The Metallurgical Society, AIME.

Poirier, D. R. 1987 *Metallurg. Trans.* B **18**, 245.

Sample, A. K. & Hellawell, A. 1982 *Metallurg. Trans.* B **13**, 495–501.

Sample, A. K. 1984 M.S. thesis, Michigan Technological University.

Sample, A. K. & Hellawell, A. 1984 *Metallurg. Trans.* A **15**, 2163–2173.

Sarazin, J. R. & Hellawell, A. 1988 *Metallurg. Trans.* A **19**, 1861–1871.

Sarazin, J. R. 1990 Ph.D. thesis, Michigan Technological University.

Scheil, E. 1942 *Z. Met.* **34**, 70.

Schmitt, R. W. 1983 *Phys. Fluids* **26**, 2373–2387.

Schreinemakers, F. A. H. 1898 *Z. Phys. Chem.* **27**, 95.

Sharp, R. M. & Hellawell, A. 1972 *J. Crystal Growth* **12**, 261.

Simpson, M., Verebaken, M. & Flemings, M. C. 1985 *Metallurg. Tran.* A **16**, 1687–1689.

Smithells, C. J. & Brandes, E. A. 1976 In *Metals reference book*, 5th edn, pp. 241–290. London: Butterworths.

Spera, F. J. 1980 In *Physics of magmatic processes*, pp. 265–323. Princeton University Press.

Stern, M. E. 1960 *Tellus* **12**, 172–175.

Stern, M. E. 1969 *J. Fluid Mech.* **35**, 209.

Turner, J. S. 1973 *Buoyancy in fluids*, ch. 8. Cambridge University Press.

Turner, J. S. 1985 *Rev. Fluid Mech.* **17**, 11–44.

Veronis, G. 1987 *J. Fluid Mech.* **180**, 327–342.

Voller, V. R., Moore, J. J. & Shah, N. A. 1983 *Metals Technol.* **10**, 81–84.

Received 11 May 1992; accepted 5 February 1993

PHILOSOPHICAL TRANSACTIONS OF THE ROYAL SOCIETY A MATHEMATICAL, PHYSICAL & ENGINEERING SCIENCES

PHILOSOPHICAL TRANSACTIONS OF THE ROYAL SOCIETY A MATHEMATICAL, PHYSICAL & ENGINEERING SCIENCES

PHILOSOPHICAL TRANSACTIONS OF THE ROYAL SOCIETY A MATHEMATICAL, PHYSICAL & ENGINEERING SCIENCES

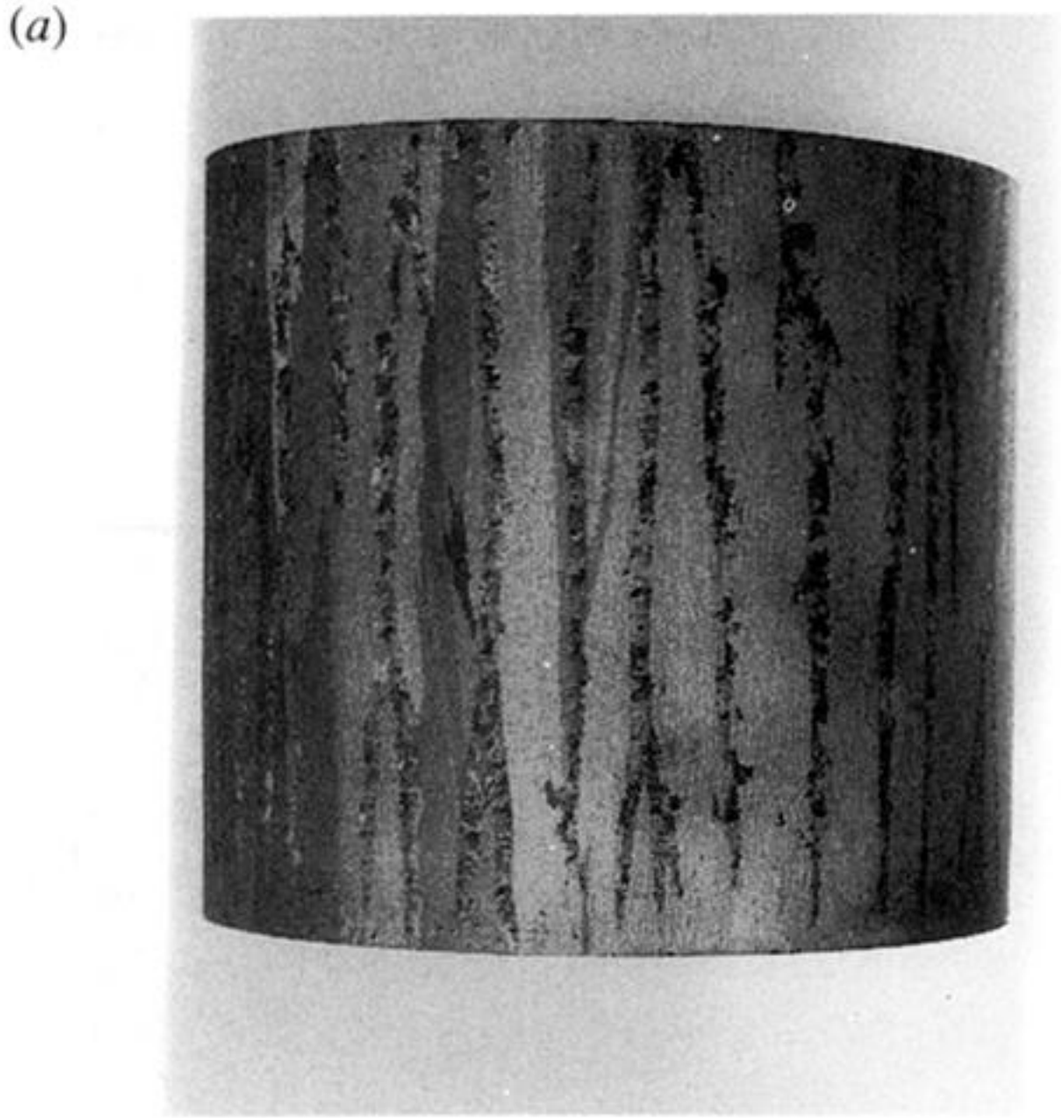

Figure 1. Deeply etched surface of a directionally solidified, superalloy ingot showing severe 'freckle' formation, (*a*) macroscopic view and (*b*) detail. Courtesy A. F. Giamei, United Technologies Research Center.

Downloaded from rsta.royalsocietypublishing.org

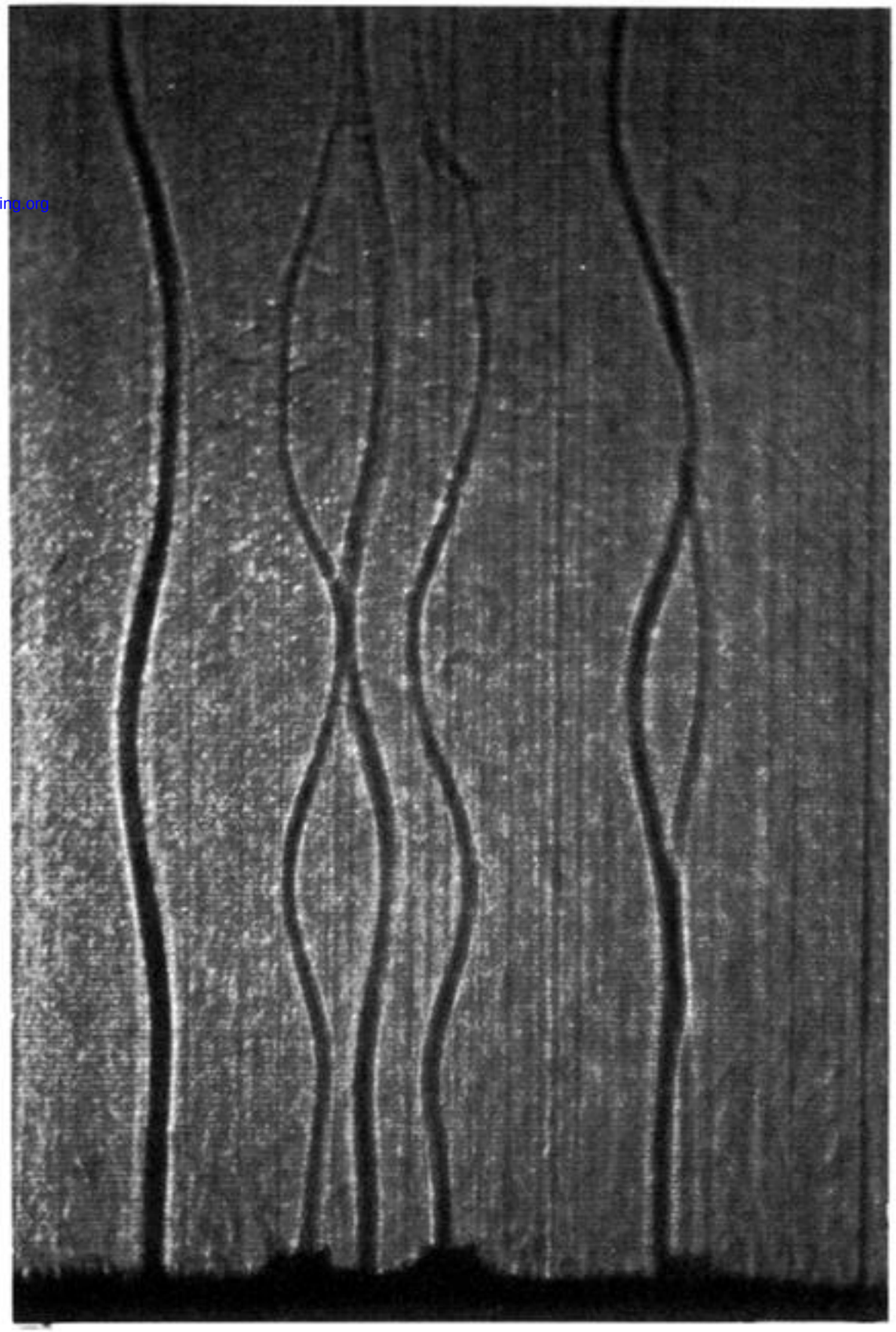

Figure 4. General view of plumes in NH_4Cl–70 wt % H_2O soon (*ca.* 20 min) after their formation. Width of cell is 48 mm. Vertical streaks are from acrylic mould.

PHILOSOPHICAL TRANSACTIONS OF THE ROYAL SOCIETY A MATHEMATICAL, PHYSICAL & ENGINEERING SCIENCES
PHILOSOPHICAL TRANSACTIONS OF THE ROYAL SOCIETY A MATHEMATICAL, PHYSICAL & ENGINEERING SCIENCES

Downloaded from rsta.royalsocietypublishing.org

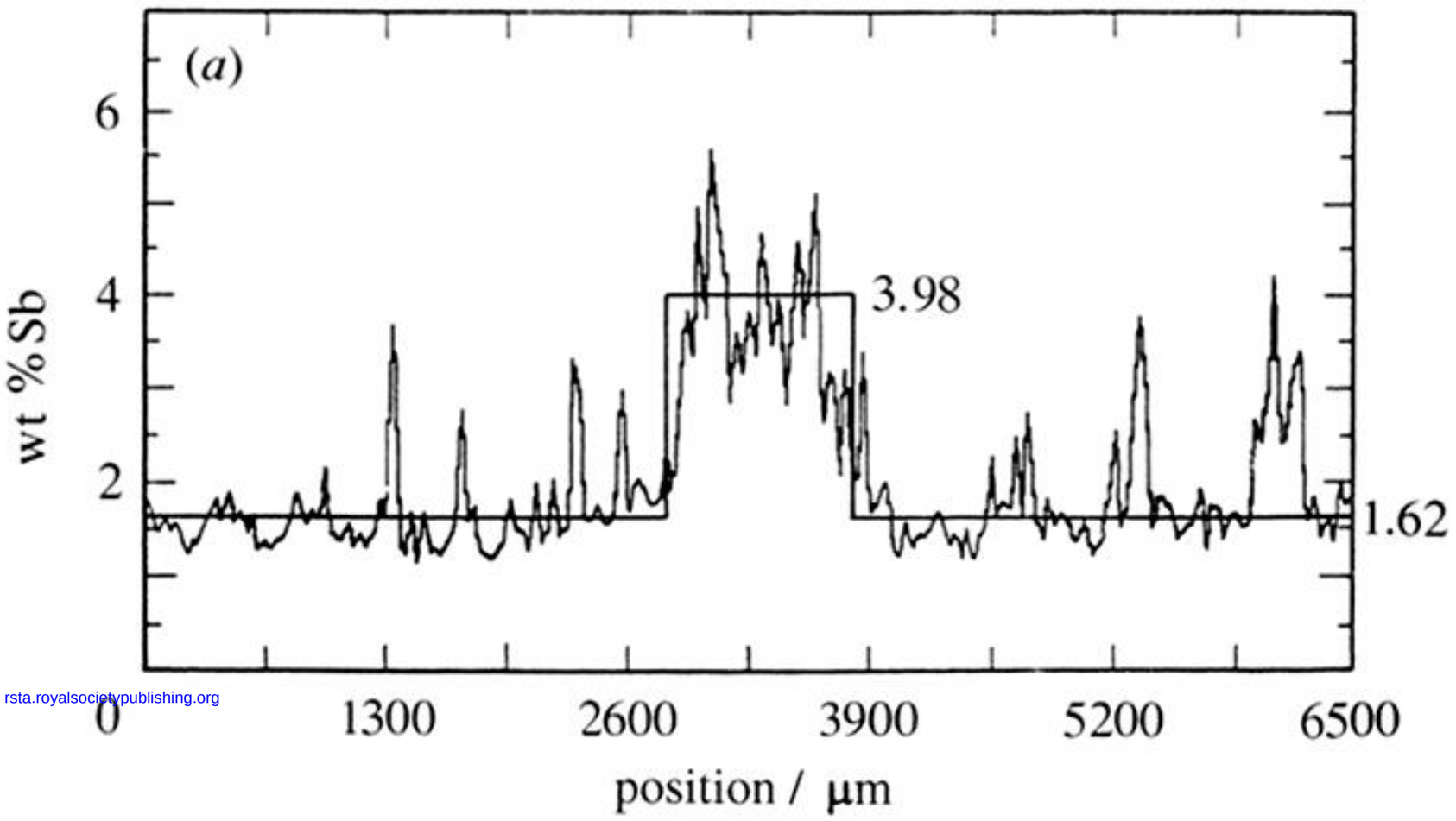

Figure 8. (*a*) EMPA area scan across a segregation channel in a Pb–2 wt % Sb sample, and (*b*) the corresponding back scatter image showing pockets of eutectic material and the line scan traces at 33 μm intervals.

PHILOSOPHICAL TRANSACTIONS OF THE ROYAL SOCIETY A MATHEMATICAL, PHYSICAL & ENGINEERING SCIENCES

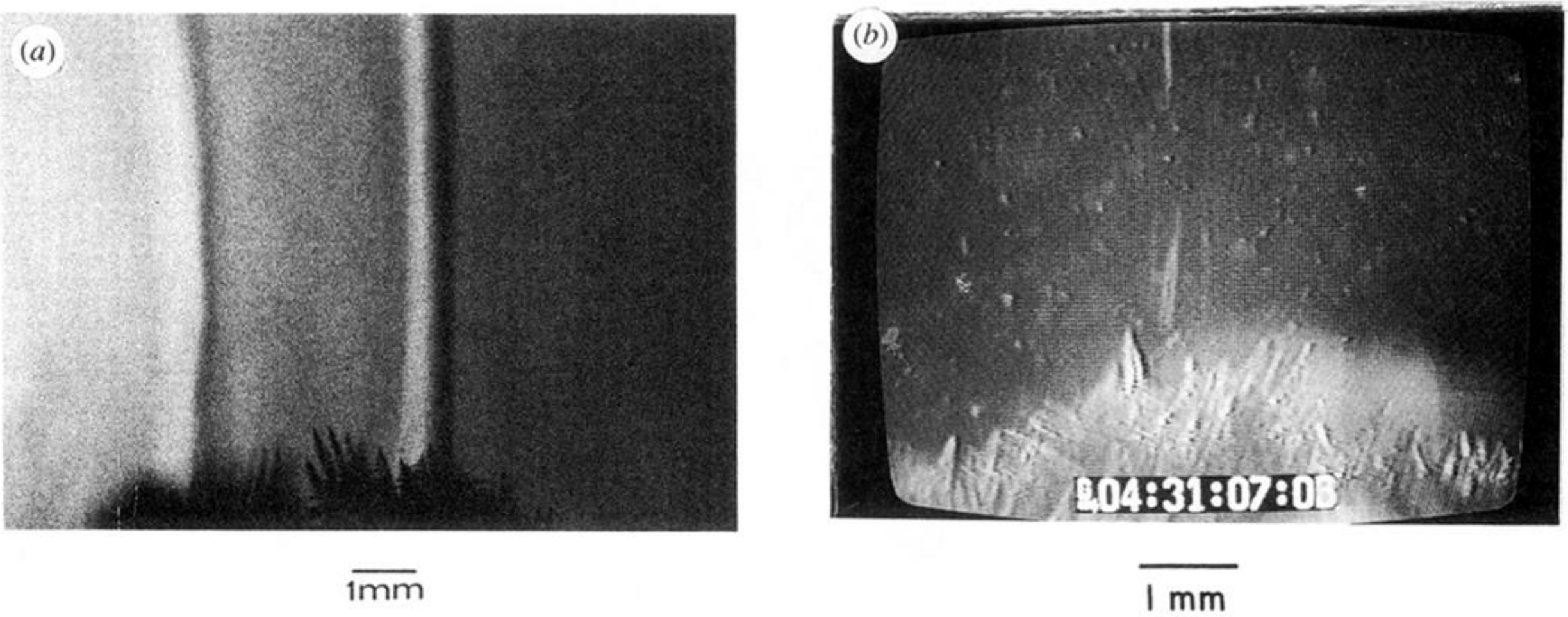

Figure 9. Channel mouth(s) with concomitant plume flow in a NH_4Cl–70 wt% H_2O casting after *ca.* 1 h; (*a*) light field image and (*b*) dark field image from video screen. In (*a*), the plumes (two, adjacent) are distinguished by sharp, concentration-dependent steps in refractive index; in (*b*), plume flow is detectable by particulate trajectories.

PHILOSOPHICAL TRANSACTIONS OF THE ROYAL SOCIETY A MATHEMATICAL, PHYSICAL & ENGINEERING SCIENCES

Downloaded from rsta.royalsocietypublishing.org

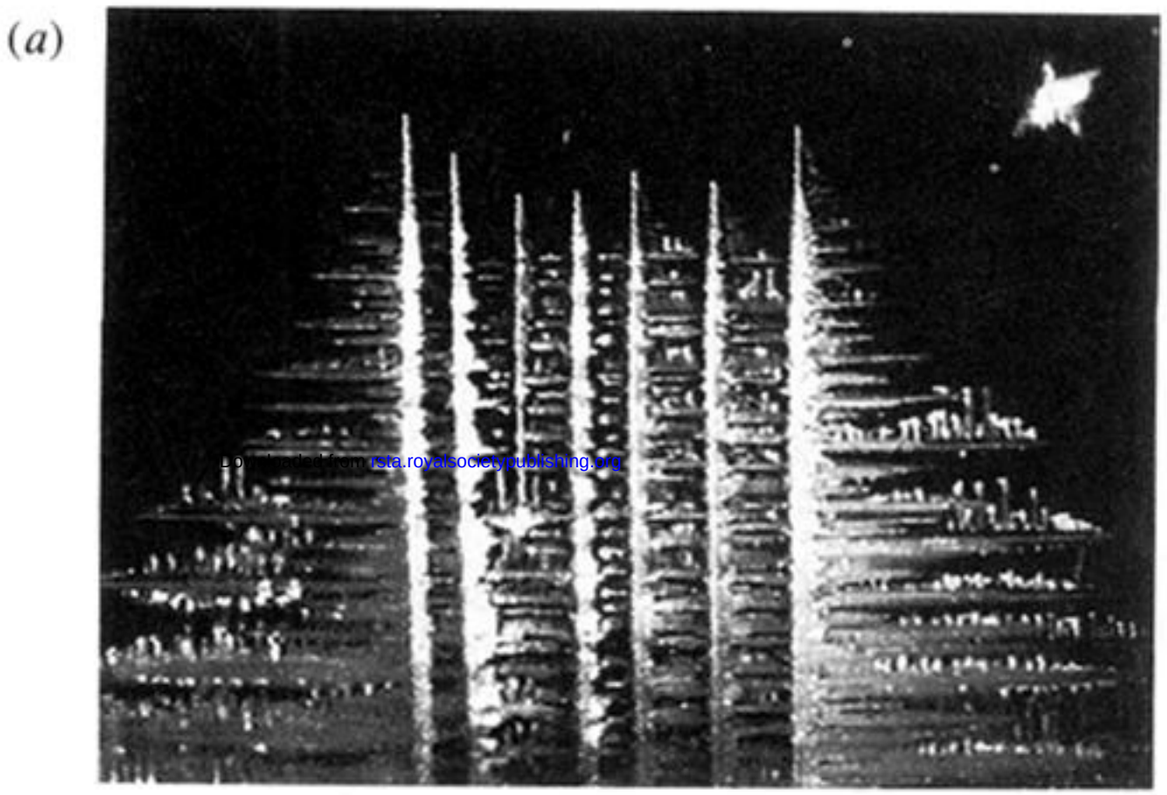

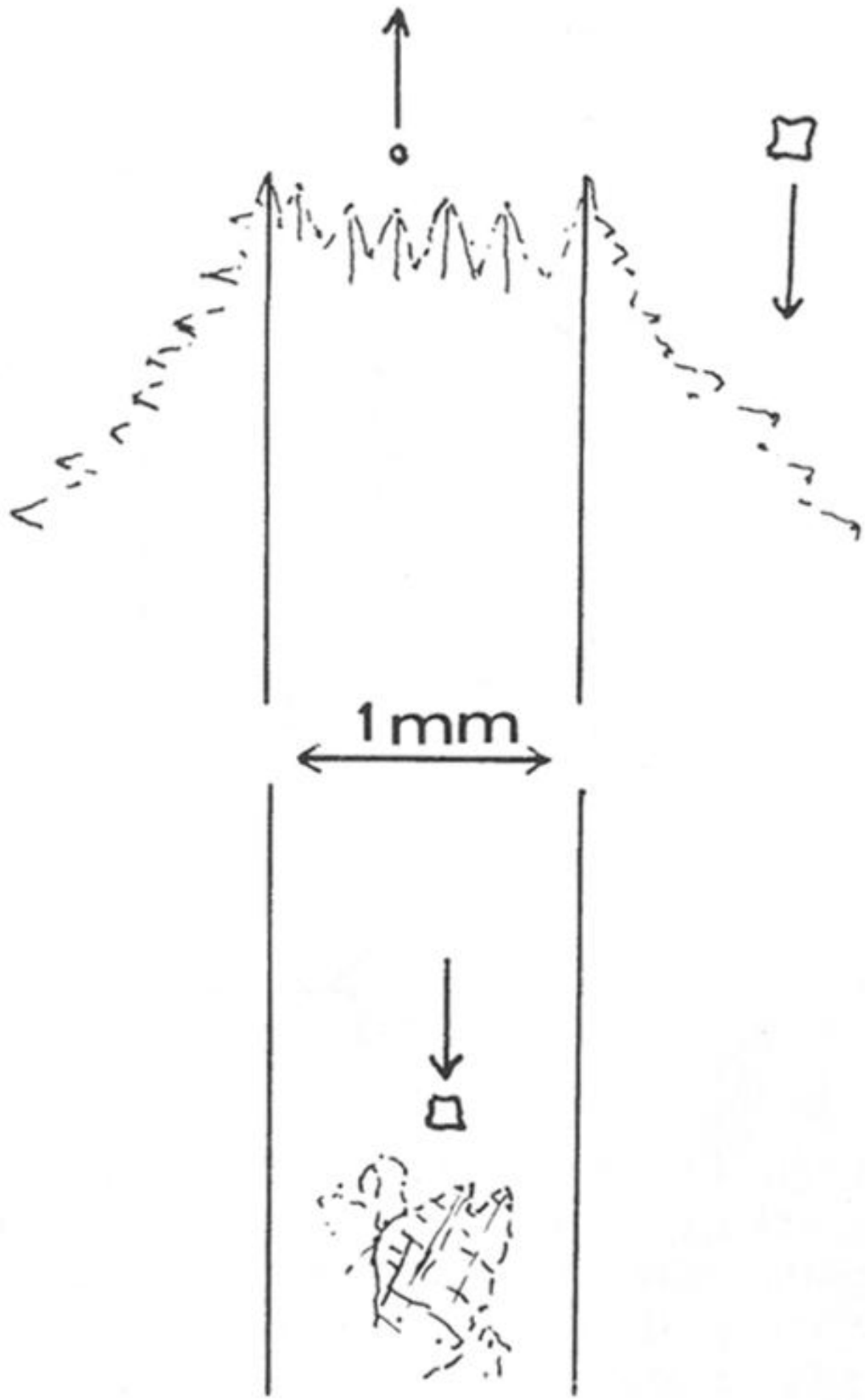

Figure 20. Taken from video frames of a channel in NH_4Cl–70 wt% H_2O which formed against the transparent mould wall, (*a*) at the mouth of the channel and (*b*) 8–10 mm lower in the mushy region. At the upper level (*a*), flow is upwards and a dendritic fragment is being ejected; in (*b*), the liquid is quiescent and a particle is sinking to accumulate as debris within the channel. Refer also to figure 1.

PHILOSOPHICAL TRANSACTIONS OF THE ROYAL SOCIETY A MATHEMATICAL, PHYSICAL & ENGINEERING SCIENCES

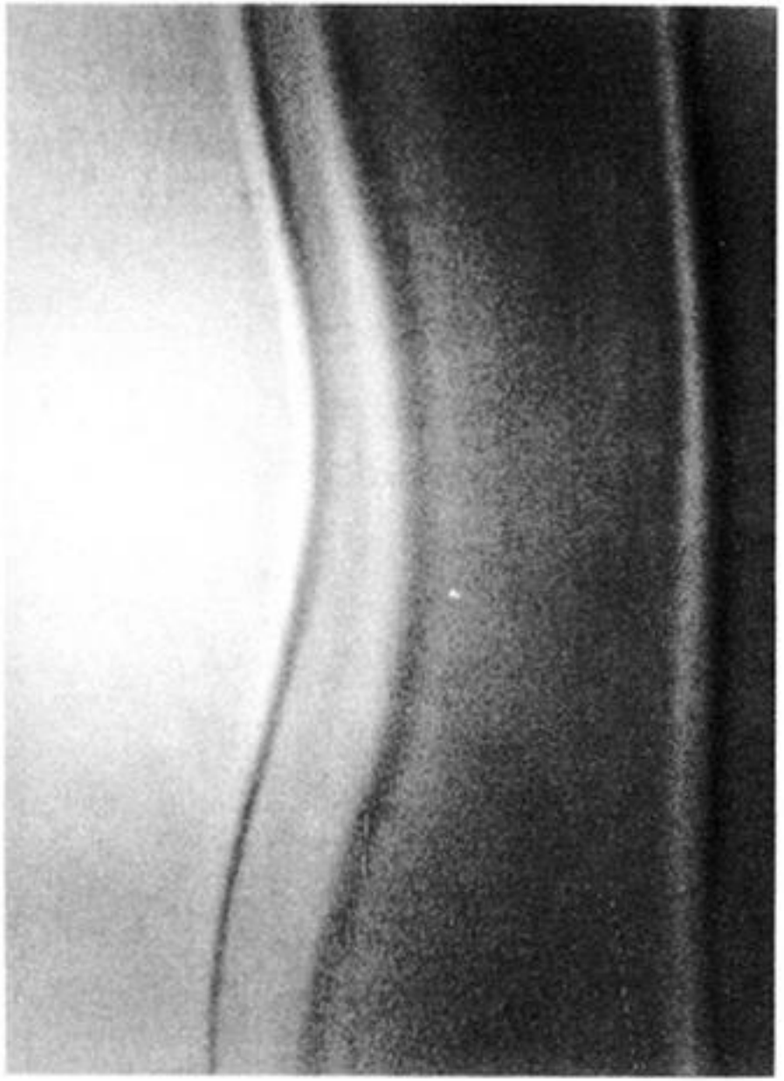

Figure 23. Synchronized helical flow in adjacent plumes, 'light field'. NH_4Cl–70 wt% H_2O, at a mean height of *ca.* 70 mm above growth front after 60 min.

PHILOSOPHICAL TRANSACTIONS OF THE ROYAL SOCIETY A MATHEMATICAL, PHYSICAL & ENGINEERING SCIENCES
PHILOSOPHICAL TRANSACTIONS OF THE ROYAL SOCIETY A MATHEMATICAL, PHYSICAL & ENGINEERING SCIENCES